Applied Energy 357 (2024) 122431

Contents lists available at ScienceDirect

Applied Energy

journal homepage: www.elsevier.com/locate/apenergy

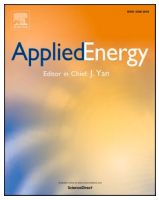

Energy, exergy, economic and environmental (4E) analysis of a cryogenic carbon purification unit with membrane for oxyfuel cement plant flue gas

Alexis Costa [a], Diederik Coppitters [b], Lionel Dubois [c], Francesco Contino [b], Diane Thomas [c], Guy De Weireld [a,*]

[a] Thermodynamics and Mathematical Physics Unit, Université de Mons (UMONS), Place du parc 20, 7000 Mons, Belgium
[b] Institute of Mechanics, Materials and Civil Engineering (iMMC), Université catholique de Louvain (UCLouvain), Place du Levant, 2, 1348 Louvain-la-Neuve, Belgium
[c] Chemical and Biochemical Process Engineering Unit, Université de Mons (UMONS), Place du parc 20, 7000 Mons, Belgium

HIGHLIGHTS

- Study of hybrid CO_2 capture system combining cryogenic and membrane technologies.
- 4E analyses considering recovery, energy consumption, exergy yield and capture cost.
- Maximum exergy efficiency for the cases where the CO_2 recovery is above 90%.
- High sensitivity of the electricity price on the CO_2 capture cost.
- Uncertainty quantification of modelling assumptions and impact on 4E analyses.

ARTICLE INFO

Keywords:
Carbon purification unit
Carbon capture
Optimisation
Economics
4E analysis
Uncertainty analysis

ABSTRACT

The carbon capture, utilisation and storage (CCUS) process chain is subject to increasing interest, and its overwhelming implementation on the industrial scale appears to be one of the main ways to reduce CO_2 emissions. In this context, the optimisation of a CO_2 purification process for oxy-combustion cement plant flue gases is proposed. This optimisation is based on a multidimensional study on the energy, exergy, economy, and environmental impacts of the process. The results of the optimisations carried out show that it is more favourable to increase the CO_2 recovery above 90%, from an energy, exergy and economic point of view. The analysis of the evolution of the capture cost as a function of the CO_2 recovery shows that for a given carbon tax, there is a minimum for the total cost which includes the sum of the carbon tax contributions for the uncaptured CO_2 and the capture cost. As the unit uses only electrical energy, the cost and the electricity generation will directly impact the capture cost as well as the overall balance in terms of CO_2 avoided. As the electricity price increases from 50 to 250 €/MWh, the CO_2 capture cost increases by almost 250%. An analysis of the parameter uncertainties allows to observe their impacts on the results, and to define a standard deviation from the optimised points and show the robustness of these. Considering the technical parametric uncertainties, the standard deviation on the electrical consumption (3.65 kWh/t_{CO2}), CO_2 recovery (0.09%) and exergy efficiency (0.92%) is limited.

1. Introduction

In order to achieve carbon neutral emissions by 2050, carbon capture, utilisation and storage (CCUS) is being developed, especially to reduce the carbon impact of industries. In various scenarios defined by the European Union to limit global warming to 1.5 °C, CO_2 capture technologies must be use and could reduce emissions by up to 40% [1]. CO_2 captured from industrial emitters can be used either directly (food-grade CO_2 for soft drinks, Enhanced Oil Recovery (EOR), supercritical CO_2 solvent, etc.) or indirectly by chemical transformation processes (methane, methanol, etc.) or for biological processes (microalgae) [2]. After ratification of the Kyoto Protocol in 1997, the European Union established an Emissions Trading Scheme (EU-ETS) for industrial installations. The system applies to large installations (with a thermal

* Corresponding author.
E-mail address: guy.deweireld@umons.ac.be (G. De Weireld).

https://doi.org/10.1016/j.apenergy.2023.122431
Received 20 July 2023; Received in revised form 18 October 2023; Accepted 27 November 2023
Available online 12 December 2023

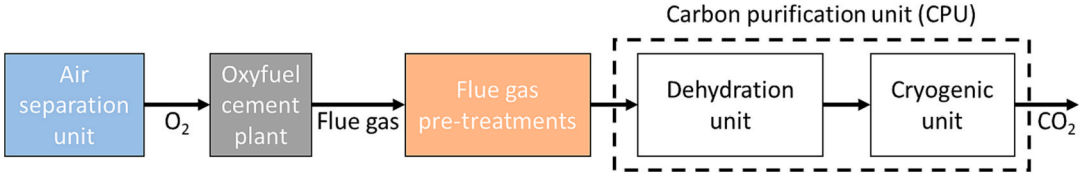

Fig. 1. Block diagram of an oxy-combustion cement plant comprising a Carbon Purification Unit (CPU).

Table 1
Literature review for CPU.

	Cold box number	Purity equipment	CO_2 in (dry)	Outlet pressure	Recovery	Purity	Electrical consumption
			mol%	Bar	%	%	kWh/t_{CO2}
[19]	3	2 Flash	75.70	110.00	90.30	95.17	164.00
[23]	2	2 Flash	75.70	110.00	91.80	96.60	136.50
[20]	1	2 Flash	75.70	97.00	90.10	96.74	N/A
[16]	1	1 Flash + Distillation	77.40	120.00	90.00	99.98	172.00
	2	2 Flash	77.40	120.00	92.00	97.54	150.00
	0	2 Flash	77.40	120.00	97.00	92.55	158.00
[21]	1	1 Flash	78.40	103.45	89.60	96.80	148.00
	1	Distillation	78.40	103.45	88.20	99.90	164.00
[17]	2	2 Flash	82.40	18.40	94.00	96.91	116.00
[18]	2	2 Flash	94.10	110.00	99.30	96.00	112.60
	1	1 Flash + Distillation	94.10	110.00	96.20	99.99	126.20

capacity of >20 MW), including those operating in industry, power generation and aviation since 2012.

European annual emissions are capped to achieve targets. CO_2 emitters concerned by the EU-ETS must buy allowances representing one tonne of CO_2 equivalent. The legislation has been changed, with an increase in the price of allowances from November 2020. From December 2021 until today, the price of the allowance is around 80€ with a price exceeding 100 € per allowance in February 2023 [3]. In practical terms, the EU-ETS market provides an incentive for industry to move towards less polluting or non-polluting alternatives technologies, or towards CO_2 capture systems to reduce emissions.

Carbon capture is possible in different ways, which can be more or less easily integrated into an existing process. These are pre-combustion, oxy-combustion, and "end of pipe" technique as post-combustion. In pre-combustion way, fossil fuel is firstly converted into hydrogen to capture CO_2 before the combustion chamber. This process produces a gas with a CO_2 concentration from 15 to 60 mol% on a dry basis. In addition, this process allows also the gas desulphurisation before combustion, which greatly reduces the production of SOx. This technique is effective in the case of energy production, such as power plants [4], or for processes that do not emit intrinsic CO_2. Indeed, for industrial sectors (i.e. cement or lime plants), where a major part of the CO_2 emissions is linked to the decarbonation of the raw material, namely the limestone, pre-combustion carbon capture is not relevant. Oxy-combustion uses relatively pure oxygen (>95 mol%) as an oxidant to increase drastically the CO_2 concentration of the flue gas. There are two possibilities for oxy-combustion. Either the furnace can withstand the higher combustion temperatures associated with pure oxygen operation, or a partial recirculation of the flue gas (mainly CO_2 and H_2O) can be carried out to maintain combustion with 21 mol% oxygen as an oxidant [5]. Consequently, the flue gases are concentrated in CO_2 (>75 mol% on a dry basis). The CO_2 content depends on the purity of the oxygen coming from an air separation unit that can introduce a significant amount of argon, as well as on the fuel used and possible air inlets bringing in nitrogen. Finally, post-combustion is the capture of the CO_2 once generated by the process. One of the advantages of this technology is that it is applicable at the end of the flue gas treatment chain ("end-of-pipe" process) allowing the integration of a capture unit without modifying the upstream process except flue gases pre-treatment units if it is necessary. However, it requires high energy consumption due to the low concentration of CO_2 in the gaseous effluent.

Several CO_2 capture technologies are available. The most developed one is based on absorption with a chemical or physical solvent. In the case of an amine(s)-based solvent, which is the most common process, it consists of a CO_2 absorption column and a regeneration column to generate a CO_2-rich stream (conventionally CO_2 purity >98 mol%) with water and traces of amine as an impurity [6]. It is conventional to recover 90% of the CO_2 present in the flue gas, even though studies are starting to show that going up to 95% could economically make sense [7]. Thermal energy must be used to regenerate the solvent, which is mainly interesting for processes having fatal heat available. Another carbon capture technology is based on an adsorption principle using porous materials, such as zeolites, aluminas or MOFs (Metal Organic Frameworks). The technologies developed (i) Pressure Swing Adsorption (PSA) using only electrical energy for compression or vacuum in the case of a VPSA or (ii) Temperature Swing Adsorption (TSA) where thermal energy is used to regenerate the adsorbent [8]. Membrane technologies are also available to separate CO_2 from a flue gas. Separation through the membrane is achieved using a pressure gradient generated by compression of the flue gas and/or vacuuming the permeate. Polymeric membranes are the most studied in the context of CO_2 capture. Their selection is based on the Robeson line [9], which is a compromise between the selectivity (ability to separate two molecules) and the permeance (flow through the membrane) of a membrane [10]. The last of the four main capture technologies is based on a cryogenic process which allows the CO_2 to be separated from other flue gas compounds based on their different condensation temperatures. This technology is well adapted when the flue gas CO_2 content is already quite high (>70%) and when the other gases are permanent gases, which is the case when it is integrated into a Carbon Purification Unit (CPU) applied to oxyfuel flue gases, as described hereafter. Additionally, there are emerging capture processes like calcium looping [11], microalgae [12], and certain plant-based approaches, such as virgin ivy plants [13,14], among others, that are being explored as potential alternatives.

In this work, a cement plant working in oxyfuel-combustion is considered. An air separation unit (ASU) is considered to produce oxygen. Among the different capture units available in the literature, it appears that for flue gases with a CO_2 concentration higher than 70% [15], the cryogenic carbon purification unit (Fig. 1) is the most suitable technology. The principle of this process is to separate the CO_2 from the

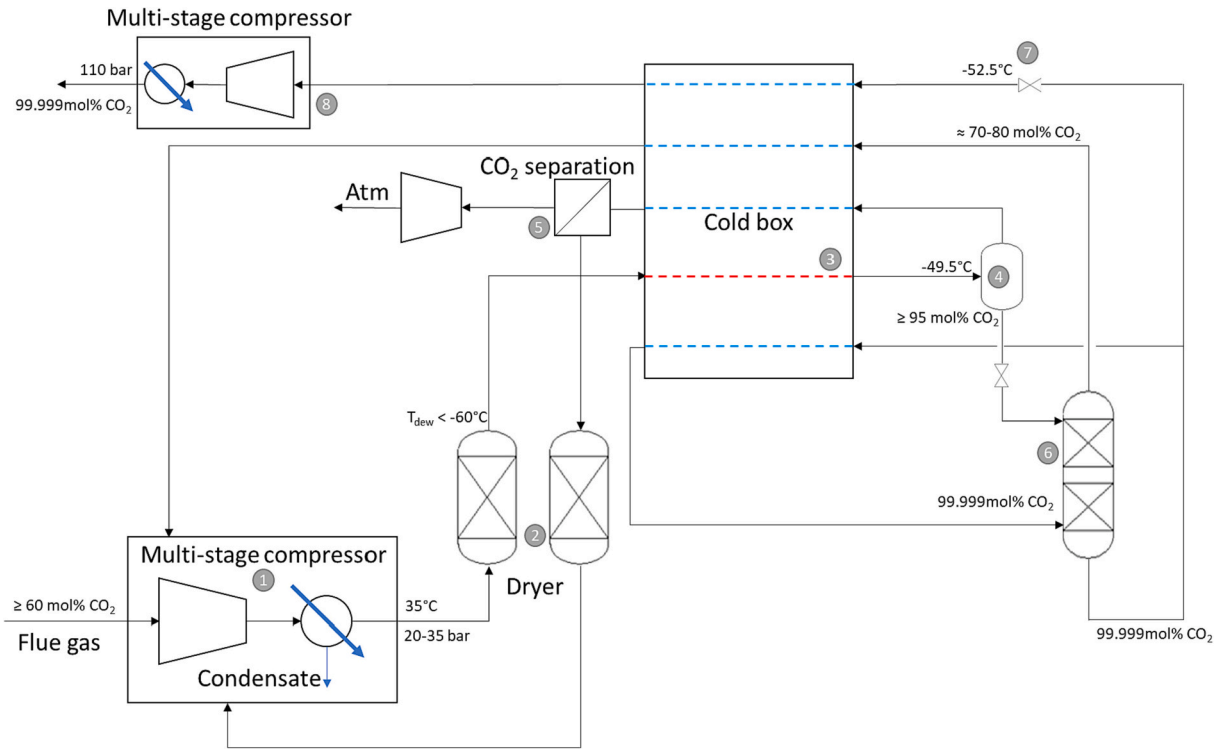

Fig. 2. CPU modelling with membrane.

other gaseous components by liquefying the carbon dioxide after dehydration and eventual flue gas pre-treatments (e.g. de-dusting, de-NOx, etc.).

Various research studies have been conducted on cryogenic carbon purification units. These studies have investigated different methods of purifying CO_2 including processes to reach medium and high purity (containing >95 mol% and 99 mol% of CO_2, respectively). The main difference between both processes is the presence of a distillation or desorption column to have a higher purity in place of several flashes for the CO_2 separation. Multi-parameter optimisation of the CPU is sought in most studies to minimise cost and/or electrical consumption.

Table 1 summarizes the relevant elements for comparing different CPUs in the literature, including the number of multi-stream heat exchangers (cold box), the purity equipment (flash, distillation or desorption column), fixed parameters such as CO_2 flue gas concentration and outlet pressure as well key performance indicators such as purity, recovery and electrical consumption. Based on the CPU with two cold boxes and two flashes illustrated by Kolster et al. [16], Jin et al. [17] and Magli et al. [18], higher CO2 purity requires more electrical consumption, while higher inlet CO2 concentration leads to greater CO2 recovery and lower electrical consumption.

Various authors [17,19,20] have studied the dynamic behaviour of a CPU to avoid the formation of dry ice due to a drop in temperature below the triple point. All three studies concluded that the most critical stream is the one related to the cooling generation following a Joule-Thompson expansion. Others have conducted techno-economic analyses, showing capture costs [21] and impacts on clinker costs [18]. Integration of CPUs into power plants reduces efficiency and increases electrical consumption [16].

Additionally, studies have optimised power consumption in two-flash, two-cold-box CPUs for treating coal-fired power plant flue gas, considering exergy destruction and "exergoeconomic" analysis [17,22]. Decreasing oxygen purity from the ASU can increase CPU power consumption but reduce overall electrical consumption in both processes [23].

The purity of the CO_2 depends on its utilisation. On the one hand, it can be transported for storage or use outside the capture site. Depending on the means of transport, whether pipeline, ship, train or truck, the characteristics of the CO_2 are more or less constrained. On the other hand, CO_2 can be used directly. In this case its specification will depend on the process (e.g. the catalyst used in a CO_2 conversion process could experience deactivations due to certain compounds, risk of corrosion, etc.). In this work, the objective is to consider a very restrictive case which corresponds to the specification given by the Northern Lights project, world's first open-source CO_2 transport and storage infrastructure, [24] for transport by ship to a terminal in western Norway for intermediate storage, before being transported by pipeline for permanent storage in a reservoir 2600 m under the seabed.

In this work, a CPU capable of generating a high purity CO_2 is modelled. In addition, to reduce the electrical consumption of the system, which directly influences the process operation costs, a hybrid system with a membrane is studied. This configuration also increases the maximum CO_2 recovery of the process compared to a standard one for a similar flue gas. The modelling of a CPU with membrane and its optimisation is addressed in the present work. Moreover, in a multi-dimensional study, an energy, exergy, economic and environmental (4E) analysis is carried out by considering an oxy-combustion flue gas coming from a cement plant as a base case. In addition, a further analysis of the source and electricity price in the system is performed. The CPU performance is subjected to a considerable number of uncertain parameters. In this framework, uncertainty quantification (UQ) allows the uncertainty on a quantity of interest to be quantified (e.g., the electrical consumption) with respect to the random environment (e.g., the compressor efficiency). Finally, a variation of the CO_2 content linked to the possibility of a higher or lower air entrance is also considered.

2. Details and design of the carbon purification unit

2.1. Process configuration

The process investigated in this work and simulated using Aspen Plus® V14 software is partly based on the Callide oxyfuel project with a CPU pilot [15,25,26]. The process combines a membrane unit to

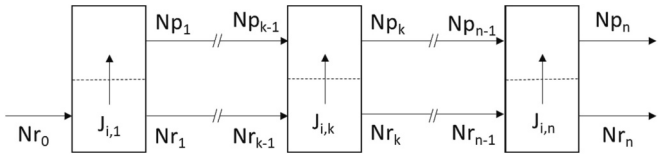

Fig. 3. Co-current membrane discretisation.

Table 2
Permeabilities of polyimide membrane studied by [33].

Molecules	CO_2	O_2	Ar	N_2
Permeability (barrer)	11	2.4	2.4	0.41

increase the CO_2 recovery with a cryogenic unit to reduce the power consumption of the compressors (lower pressure) and, at the same time, a compression unit for sending the CO_2 in a supercritical state into a pipeline. The flue gases treated are produced by an oxy-combustion cement kiln.

Fig. 2 represents the investigated CPU system. It can be divided into eight subsystems: (1) flue gas compression, (2) flue gas drying, (3) flue gas cooling, (4) CO_2 vapour-liquid separation, (5) CO_2 recovery of the vapour from flash, (6) CO_2 purification, (7) cold generation and (8) CO_2 compression.

The objective of the cryogenic unit is to cool the flue gas to recover CO_2 with high purity. This cooling is applied close to the triple point temperature for pure CO_2 (−56.6 °C) but without going below it to avoid any dry ice in the installation. A limit of −54 °C is fixed to avoid any issues with the triple point. The flue gas enters the multistage compression chain to reach the working pressure, allowing at least 90% CO_2 recovery (1). The gas is compressed in 3 compressor stages to get the compression ratio between 2 and 5 by stage, and to limit gas warming below 200 °C [27]. The stream is dried by an adsorption column containing silica gel or alumina to a dew point temperature below −60 °C (2). The stream is then cooled in the cold box before entering the flash at −49.45 °C. The multi-stream heat exchanger technology is a brazed aluminium heat exchanger (BAXH) that was demonstrated in the Callide project [26] (3). The cooled flue gas is sent to a flash to separate liquid CO_2 from the incondensable gases (4). The cold duty of the vapour phase coming from the flash is recovered in the cold box, before being sent to the membrane to recover CO_2 that will be used to regenerate the dryer and being recirculated through multistage compression. The non-condensables are expanded in a turbine (5). The desorption column extracts the impurities of the liquid CO_2 coming from the flash by means of a pure CO_2 vapour (6). The desorption of impurities allows a CO_2 purity of 99.999 mol% to be reached. The liquid obtained at the bottom of the column is separated into two streams. The first one is heated to generate the CO_2 vapour used in the column. The second one is expanded in a Joule-Thomson valve (7) to generate a stream at −52.45 °C to obtain a pinch of 3 °C with the stream to be cooled [28]. At the end of this process, the CO_2 is compressed in order to be injected into the pipeline distribution at 110 bar (8).

2.1.1. Membrane modelling

The membrane is a unit operation that is not available in Aspen Plus® V14. To integrate this separation process, it has been developed in Aspen Custom Modeler™ V14. The validation of the model is available in the supporting information section I.1. The membrane has been discretised into different slices following the works of Fanchon [29] and Fernandes Rodrigues [30]. Temperature variations are taken into account according to the Joule-Thomson effect. A relationship between the permeate and feed temperatures has been proposed by Gorissen [31].

To model the membrane, several assumptions are made in this work:

- there is no gradient of concentration in each discretisation slice;
- the membrane is co-current;
- there is no pressure drop along the membrane;
- the permeability is constant;
- the transfer is done by diffusion through a non-porous membrane.

The co-current membrane is schematically presented on Fig. 3. The equations related to the system are the total and partial molar balances for the slices and the permeate. These equations are described hereunder:

- Diffusion through a non-porous membrane

$$J_i = \frac{P_i(p_{Ri} - p_{Pi})}{e} \tag{1}$$

Global molar balance per slice

$$Nr_{k-1} + Np_{k-1} = Nr_k + Np_k \tag{2}$$

- Global molar balance on the permeate side

$$Np_{k-1} + \sum_i J_{i,k}A_k = Np_k \tag{3}$$

- Partial molar balance per slice

$$Nr_{k-1}y_{ri,k-1} + Np_{k-1}y_{pi,k-1} = Nr_k y_{ri,k} + Np_k y_{pi,k} \tag{4}$$

- Partial molar balance on the permeate side

$$Np_{k-1}y_{pi,k-1} + J_{i,k}A_k = Np_k y_{pi,k} \tag{5}$$

where J_i is the diffusion flux (mol/(m^2 s)), P_i is the permeability (mol m/(m^2 Pa s)), p_{Ri} and p_{Pi} are the partial pressure of the retentate and permeate side respectively (Pa), e is the membrane thickness (m), Nr_k is the retentate molar flux out of the slice k (mol/s), Np_k is the permeate molar flux out of the slice k (mol/s), A_k is the membrane area of the slice k (m^2) and $y_{pi,k}$ and $y_{ri,k}$ are the molar fractions for the component i in the slice k (−) for permeate and retentate respectively.

The characteristic parameters of the membrane units are the surface, thickness, and permeability of the molecule through the membrane. The ratio between the permeability and thickness gives the permeance. The operating parameters from the process are the composition, temperature and pressure of the feed and the pressure on the permeate side.

Many papers have studied different types of membranes for the separation of carbon dioxide/nitrogen, which are the two major components in the CO_2 capture process but in this case, oxygen and argon must be also considered. When the permeability is plotted as a function of selectivity (ratio between permeability of two molecules), there is a limit called the Robeson limit [9] implying that the membranes have a maximum selectivity which decreases as the permeability increases. Hence a membrane close to the Robeson limit will have the best selectivity for a given permeability. In this case the selectivity must be high enough to reduce the recirculation of non-condensables and then to limit the electrical consumption by their presence, but the permeance must not be also too low to keep a reasonable surface area. There is a trade-off between increasing CO_2 recovery and decreasing electrical consumption and the membrane cost.

Currently, commercial membranes are mainly used for natural gas purification. Air Liquide has developed a MEDAL™ membrane (based on polyimide) [32] which has properties close to those studied by Hao et al.

Table 3
Compositions of an outcoming gas from an oxyfuel cement industry (simulation –courtesy of ECRA).

Components	Molar composition
CO_2	79.0%
N_2	9.9%
O_2	2.9%
Ar	1.2%
H_2O	7.0%

[33]. The permeabilities of the membranes are given in Table 2. These inputs are considered in this work for the membrane separation with a thickness of 1 μm.

2.1.2. Process modelling

The flue gas treated in this work comes from an oxy-combustion cement kiln, based on a production of 3000 $t_{clinker}$/day. These data are based on simulations carried out by the European Cement Research Academy (ECRA). Table 3 summarizes the composition of the flue gas to be treated. The flue gas is cooled down to 40 °C and considered to be cleaned from dust, SO_x and NO_x. To clean the flue gas and reduce them to a few ppm, various processes can be employed [15]. These include a Sour Compression Unit (SCU) [34,35], a NaOH column [26], or more conventional methods like Selective Catalytic Reduction (SCR) [36] and processes using lime [37]. Particulate matter is typically removed using electrostatic precipitators or baghouse filters [38]. Moreover, this clinker production corresponds to a flow rate of 70,000 Nm^3/h. In this way, the flue gas contains 116.89 t_{CO2}/h. The relatively high presence of nitrogen is explained by taking account of air intrusion in the model. Argon is introduced simultaneously with O_2 as an impurity from the air separation unit.

Modelling in Aspen Plus® V14 software was performed (Fig. 4). The predictive Peng-Robinson 1978 (PPR78) equation of state [39] was chosen to determine the thermodynamic properties of the fluid mixture. Temperature-dependent k_{ij} were considered [40] (group-interaction parameters for CO_2–N_2 determined by Privat et al. [41] and CO_2-O_2 and CO_2-Ar by Xu et al. [42]. The validation of the implementation of the thermodynamic model in Aspen Plus is detailed in Section I.2 of the supporting information.

The flue gas was at 1 atm and 40 °C. The centrifugal compressors were designed with an isentropic efficiency of 85% and the stream was cooled to 35 °C after each compression step before the purge of the condensate. The permeate (PERM) pressure was set at the pressure of the compressor (C1) considering the pressure drops inside the heat exchanger. The retentate (RET) is heated with the heat release of (COMP2) by keeping a

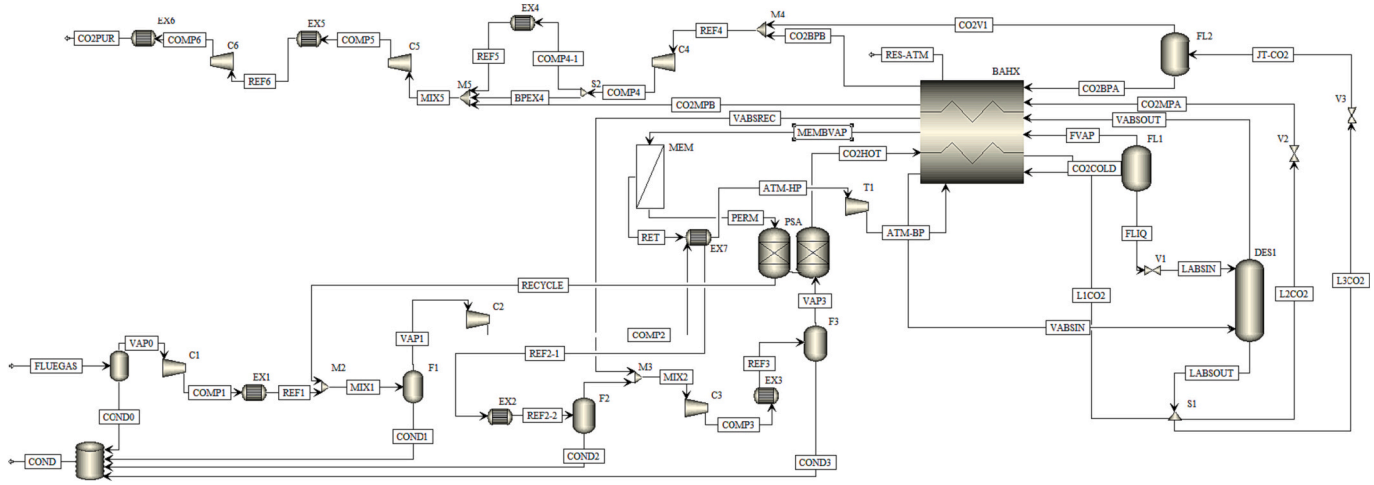

Fig. 4. Aspen flowsheet of the CPU.

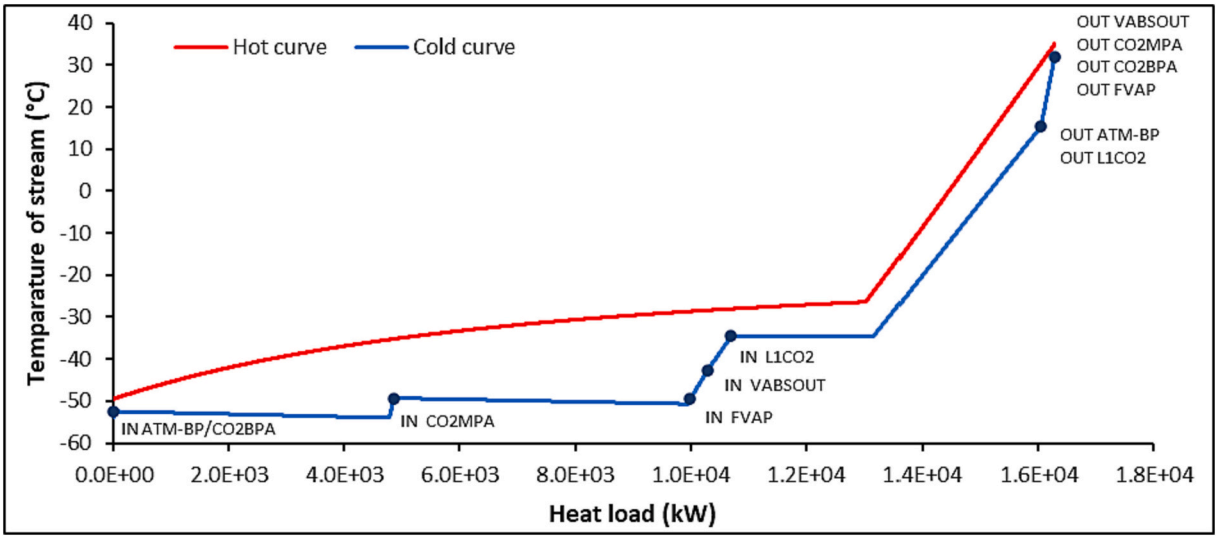

Fig. 5. T-Q diagram of multi-stream heat exchanger (BAHX).

Table 4
Reference environment (25 °C, 1 atm) [47].

Components	Molar composition
O_2	20.54%
N_2	76.34%
Ar	0.913%
H_2O	2.17%
CO_2	0.0337%

pinch of 40 °C. As such, the expansion of (ATM-HP) was more efficient thanks to the increase of the stream temperature. The temperature at the outlet of (T1) is set to −54 °C. The outlet pressure of (C2) was set in function of the desorption column (DES1) pressure considering pressure drops in the BAHX and in the heat exchanger. The temperature minimum in the multi-stream heat exchanger was also set to −54 °C. The desorption column was modelled thanks to a Rad-Frac model using the rate-base mode. A Mellapak 250Y from Sulzer© was used as structured packing in the column. The outlet pressure of the compressor (C4) was set to the pressure of the valve (V2) minus the pressure drops from BAHX. The valve (V2) was a second Joule-Thompson expansion to reduce the flowrate through the compressor (C4) coming from the first Joule-Thompson expansion in the valve (V3). The vapour from this expansion was mixed with the vapour coming from the liquid phase of the same stream to reduce the stream temperature (REF4) and therefore to improve the compression efficiency. A by-pass (BPEX4) was modelled in the case that the temperature after this compression was less than the minimum temperature required to cool the stream.

Fig. 5 illustrates the heat exchange through a T-Q diagram between the cold streams and the hot stream. The stream with the lowest temperature is ATM-BP, which is quickly joined by the stream (CO2BPA) that has been expanded in V3. Following this is the duty of the CO2MPA stream from the second Joule-Thompson expansion, which is maintained at a higher pressure and thus generates a liquid-vapour stream at a higher temperature. The Joule-Thompson expansion streams contribute to nearly two-third of the duty required for cooling and partial liquefaction of the flue gas. The remaining duty is provided by FVAP, VABSOUT, and L1CO2, with only the latter being in the liquid phase at the inlet of the exchanger, allowing for the recovery of its latent heat to complete the necessary duty for the phase change of the flue gas.

The dryer considered in this work applies a Pressure Swing Adsorption (PSA) process and beds are filled with silica gel. The adsorption pressure was in the range of the compressor (20–35 bar) and the desorption pressure was in the range of the permeate pressure (2–5 bar). Rezk et al. [43] presented a complete study about silica gel as a desiccant. Based on the 2-bed cycle, an adsorption time of 10 min is considered with the same duration for the regeneration step. The quantity of water adsorbed can be calculated thanks to isotherms equations. From the flowrate of the stream to dry, the adsorption time, the packed bulk density (1000 kg/m^3) and the molar adsorption loading allow the calculation of the adsorbent volume.

The pressure drop in the cold box is relative to the plate-fin heat exchanger. Magli et al. [18] consider a pressure drop of 2% of the inlet pressure in the cold box. A pressure drop of 0.21 bar is taken into account by Koohestanian et al. [20]. With Aspen Exchanger Design and Rating™, the cold box can be designed from the streams calculated in Aspen Plus®. This method allows the pressure drop for a cold box design to be calculated. Considering the friction at the distributors situated at the inlet and outlet of the BAHX as well as friction along the exchanger, the pressure losses have an average value of 0.45 bar. This value was used to determine the pressure drop in the BAHX. A pressure drop of 0.2 bar was assumed for the intercooling heat exchanger.

2.1.3. Single variable analysis

A parametric study was performed and highlighted the variables that have an impact on major process performances: electrical consumption, CO_2 purity and recovery.

The pressure at the cold box inlet influences the CO_2 recovery and the purity of the liquid out of the flash. If the pressure increases, more CO_2 is recovered, but the other compounds are more solubilised in liquid phase, degrading the purity of the liquid CO_2 produced.

A higher surface area of the membrane increases the CO_2 recovery to a maximum threshold for a given permeability. A minimum energy is consumed when the surface area is larger due to the decrease in the amount of CO_2 transferred per unit area, as opposed to other compounds, such as N_2, O_2, etc., which increase the amount of incondensable gas in the permeate and, therefore, the electrical consumption.

The desorption column allows CO_2 liquid purification with pure CO_2 vapour. For a given column, a rise in the vapour flowrate increases the purity, but this implies an increase in the recirculated flow and, therefore, the energy required to increase its compression. For an increase in pressure, the purity decreases, but this reduces the energy required to compress the final product. Thus, an optimum is possible by varying these two parameters.

Considering the cold box, optimisation can be done with Joule-Thompson expansion. Minimising the energy loss between the hot and cold streams by varying the flow rate and pressure of the second stream allows the optimisation of the duty quantity to be exchanged and the temperature of the stream.

2.2. Energy balance

The energy analysis focuses, according to the first law of thermodynamics, on the amount of energy related to the process without considering the losses.

$$\sum \dot{Q} + \sum \dot{W} + \sum \dot{n}h = 0 \tag{6}$$

where $\dot{Q}$ is the heat power (kW), $\dot{W}$ is the mechanical power rate (kW), $\dot{n}$ is the mole flowrate (mol/s) and h is the enthalpy (kJ/mol).

The electrical consumption per tonne of CO_2 is often the Key Performance Indicator (KPI) parameter used to show the efficiency of a system. In a cryogenic CPU, the energy required is mainly electrical due to the consumption of the compressors.

$$E_{consumption} = \frac{\dot{W}_{FG\_C} + \dot{W}_{CO_2\_C} - \dot{W}_T}{\dot{m}_{CO_2 captured}} \tag{7}$$

where $E_{consumption}$ is the electrical consumption of the process (kWh/t_{CO2}), $\dot{W}_{FG\_C}$ is the flue gas compressor mechanical power rate (kW), $\dot{W}_{CO_2\_C}$ is the CO_2 product compressor mechanical power rate (kW), $\dot{W}_T$ is the turbine mechanical power rate (kW) and $\dot{m}_{CO_2 captured}$ is the mass flowrate of the captured CO_2 (t_{CO2}/h).

2.3. Exergy analysis

The exergy analysis is based on a combination of the first and second laws of thermodynamics to consider both the quantities of energy used and their quality, allowing the calculation of the energy useful for the work (exergy) and the energy lost and degraded during the process. The exergy comprises four terms (physical, chemical, potential and kinetic contributions). However, the last two being negligible, the exergy is calculated as follows [44]:

$$ex = ex_{ph} + ex_{ch} \tag{8}$$

where ex is the exergy (kJ/mol), ex_{ph} is the physical exergy (kJ/mol) and ex_{ch} is the chemical exergy (kJ/mol).

The physical contribution of the exergy is the amount of work obtainable by physical processes involving thermal interaction that allows the system to change from an initial state to the state of the environment (P_0 (1 atm) and T_0 (25 °C)).

Table 5
Capital cost variable of components (*: $F_p = 1$ for P < 5 barg) [48].

Equipment Type	K_1	K_2	K_3	B_1	B_2	F_{BM}	C_1	C_2	C_3
Compressors Centrifugal	2.2897	1.3604	−0.1027	–	–	2.7	–	–	–
Floating head HX	4.8306	−0.8509	0.3187	1.63	1.66*	–	0.03881	−0.11272	0.08183
Turbines	2.2476	1.4965	−0.1618	–	–	1	–	–	–
Vertical towers and vessels	3.4974	0.4485	0.1074	2.25	1.82	–	–	–	–

Table 6
Base case assumptions for OPEX (electricity from [52], labour cost from [53] and other coefficients from [48]).

Parameter	Value
Utilities (C_{UT})	Electricity: 100 €/MWh Cooling water: 15.7 $\$_{2018}/m^3$
Operating Labour Cost (C_{OL})	15 labours; 90,632 €/labour/year
Direct supervisory and clerical labour	0.18 C_{OL}
Maintenance and repairs	0.06 CAPEX
Operating supplies	0.15 (0.06 CAPEX)
Laboratory charges	0.15 C_{OL}
Patents and royalties	0.03 OPEX
Local taxes and insurance	0.032 CAPEX
Plant overhead costs	0.6 (1.18 C_{OL} + 0.06 CAPEX)
Administration costs	0.15 (1.18 C_{OL} + 0.06 CAPEX)
Distribution and selling costs	0.11 OPEX
Research and development	0.05 OPEX

$$ex_{ph} = (h - h_0) - T_0(s - s_0) \tag{9}$$

where T_0 is the environment temperature (K), s is the entropy (kJ/(mol. K)) and subscript 0 is for environmental reference state.

The chemical contribution of the exergy of a reference substance is calculated using the concentration of the compound at the reference state [45,46]. The exergy of the compounds in the atmosphere is determined by

$$ex_{ch,i} = RT_0 ln\frac{1}{y_i} \tag{10}$$

where R is the gas constant (kJ/(K mol)) and, y_i is the vapour mole fraction (−).

Table 4 provides the composition of the air for the reference state at 25 °C and 1 atm with a relative humidity of 70%, as proposed by Rivero & Garfias [47] based on the environmental reference state from Szargut [46].

When a compound is not present in the environment, the chemical exergy of the compound can be calculated by setting up a reversible reaction of formation.

$$ex_{ch,i} = -\left(\sum_{PROD}\nu_p\Delta gf_p - \sum_{REACT}\nu_r\Delta gf_r\right) + \sum_{PROD}\nu_p ex_{ch,p} - \sum_{REACT\neq i}\nu_r ex_{ch,r} \tag{11}$$

where ν is the stoichiometric coefficient (−), Δgf is the formation of Gibbs free energy (kJ/mol), and r and p subscript are for reactants and products respectively.

The chemical exergy of a biphasic liquid-vapour system is calculated as

$$ex_{ch} = (1-\omega)\sum_i x_i\left(ex_{ch,i} + \Delta G^0_{v\to l} + RT_0 ln\gamma_i x_i\right) + \omega\sum_i y_i\left(ex_{ch,i} + RT_0 lny_i\right) \tag{12}$$

where ω is the vapour fraction (−), x_i is the liquid mole fraction (−), $\Delta G^0_{v\to l}$ is the standard Gibbs energy of condensation (kJ/mol) and, γ is the activity coefficient (−).

The exergy destruction (Ex_D) represents the irreversibility of the process implying that the exergy can be partially or totally destroyed.

$$\sum \dot{n}\, ex_{in} + Ex_Q = \sum \dot{n}\, ex_{out} + Ex_W + Ex_D \tag{13}$$

The heat and work exergy described with subscripts Q and W respectively corresponds to:

$$Ex_Q = \int_{T=T_{in}}^{T_{out}}\left(1 - \frac{T_0}{T}\right)dQ \tag{14}$$

$$Ex_W = \dot{W} \tag{15}$$

The exergy efficiency (η_{ex}) of the process is a parameter calculated to evaluate its thermodynamic performance. This efficiency considers the exergy destruction as well as the loss exergy (Ex_L) (related to cooling, wastewater, and by-products) compared to the contribution of the fuel exergy (Ex_F) that is the sum of the exergy of the flue gas and the electricity supplied [17]. This parameter is expressed as:

$$\eta_{ex} = 1 - \frac{Ex_D + Ex_L}{Ex_F} \tag{16}$$

2.4. Economic analysis

The calculation method of the CAPEX (CAPital EXpenditures) and OPEX (OPerational EXpenditures) for a process is based on (Turton et al., 2018) [48].

The Chemical Engineering Plant Cost Index (CEPCI) is used as an index to consider the inflation of the equipment cost and services associated with chemical process industries.

$$C_{actual} = C_{reference}\left(\frac{I_{actual}}{I_{reference}}\right) \tag{17}$$

where C is the cost (€), and I is the index (−) with their corresponding subscripts, namely 'actual' and 'reference'. Costs are calculated with the CEPCI value relative to the year 2022 which is 816.2 [49].

Economic analysis involves the estimations of the CAPEX that can be calculated thanks to the purchased equipment cost (C_p^0), the bare module cost (C_{BM}) that includes direct and indirect costs (all associated equipment and installation labour close the purchased equipment), and the last contributions are from the contingency costs, and fees. Eqs. (18)–(21) are used to calculate the CAPEX with the parameters listed in Table 5.

$$log_{10}C_p^0 = K_1 + K_2 log_{10}(S) + K_3[log_{10}(S)]^2 \tag{18}$$

$$C_{BM} = C_p^0\left[B_1 + B_2\, F_P F_M\right] = C_p^0 F_{BM} \tag{19}$$

$$log_{10}F_{p,hx} = C_1 + C_2\, log_{10}(P) + C_3\,[log_{10}(P)]^2 \tag{20}$$

$$F_{p,vessel} = \frac{\frac{P\,D}{2\,St\,E-1.2\,P} + CA}{t_{min}} \tag{21}$$

where C_p^0 is the purchased equipment cost corresponding to the atmospheric operating pressure and using carbon steel construction, S is the size of the equipment, F_M is the material factor (1 for carbon steel material), F_P is the pressure factor, P is the pressure (bar), D is the diameter (m), t_{min} is the minimum allowable vessel thickness (0.0063 m), CA is the corrosion allowance (0.00315 m), E is the weld efficiency (0.9), St is the

Table 7
Variables for the optimisation with lower and upper bounds.

Variables	Definitions	Units	Lower bounds	Upper bounds
P_{C1}	Discharge pressure of C1 compressor	bar	2	5
P_{C3}	Discharge pressure of C3 compressor	bar	15	30
P_{V1}	Pressure of the V1 valve	bar	9	15
P_{V2}	Pressure of the V2 valve	bar	6	15
F_{L1CO2}	Mass fraction towards L1CO2	-	0.05	0.25
F_{L3CO2}	Mass fraction towards L3CO2	-	0.05	0.5
A	Membrane area	m^2	1000	200,000
H_{DES1}	Tower DES1 height	M	5	20

Table 8
Constraints for the optimisation.

Constraint	Justification
Purity ≥99.999 mol%	Fixed purity for the transport
$T_{compressor} \leq 200$ °C	Technology limitation [27]
BAHX Pinch ≥3 °C	Technology limitation [28]
$T_{stream} \geq -54$ °C	Limit to avoid dry ice formation (−56.6 °C)
$P_{V1} \leq P_{C3}$–0.045 bar	Pressure of FLIQ higher than pressure of LABSIN
$P_{V2} \leq P_{V1}$	Pressure of L2CO2 higher than pressure of CO2MPA

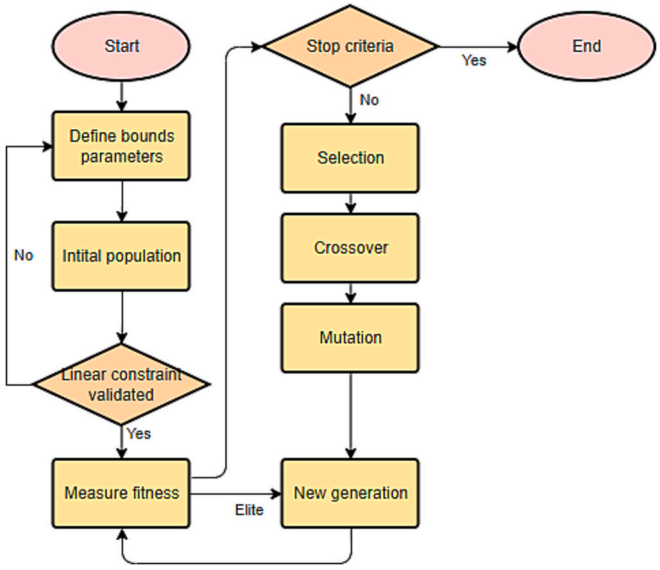

Fig. 6. Illustration of the genetic algorithm concept.

Table 9
GA configuration.

Parameters	Value
Population size	50
Crossover probability	0.2 for ≤ generation 25 0.8 for > generation 25
Pareto fraction	0.5
Constraint tolerance	10^{-4}
Function tolerance	$0.2\ 10^{-4}$
Stall generation	50

allowable stress for carbon steel (944 bar) and B_i, C_i and K_i are constants.

The membrane cost is set at 50 €/m^2 including direct and indirect costs [10] with a lifetime of five years and a replacement cost fixed at 25 €/m^2. Considering an invariable replacement cost, the total membrane cost for a 25-year plant lifetime is estimated at 150 €/m^2. The adsorbent

Table 10
Ranges considered on the uncertain parameters for uncertainty quantification and global sensitivity analysis.

	Units	Default value	Uncertainty	Distribution
FG compressor efficiency	%	85	± 5%	Uniform
CO_2 compressor efficiency	%	85	± 5%	Uniform
Turbine efficiency	%	90	± 5%	Uniform
Cooling water heat exchanger pinch	°C	10	± 3 °C	Gaussian
O_2 concentration	mol%	2.9	± 0.5%	Uniform
Permeability CO_2	barrer	11	± 10% (relative)	Gaussian
Permeability N_2	barrer	0.41	± 10% (relative)	Gaussian
Permeability O_2/Ar	barrer	2.4	± 10% (relative)	Gaussian

cost used in the dryer is fixed at 1.32 USD_{2020}/kg [50]. Aspen Economics is used to generate the BAHX cost since this equipment is not available in Turton et al. [48]. This cost is calculated thanks to the volume, itself calculated considering the overall heat-transfer coefficient being U = 170 W/m^2K [20] and the surface to volume ratio being 2000 m^2/m^3 [51].

The contingency cost varies depending on the reliability of the cost data and completeness of the process flowsheet available. This factor is included in the evaluation of the cost as a protection against oversights and poor/wrong information. Unless otherwise stated, values of 15% and 3% of the bare module cost are assumed for contingency costs and fees, respectively. Adding these costs to the bare module cost provides the total module cost.

OPEX can be calculated using various known or estimated costs (Table 6). These costs are CAPEX, Operating Labour Cost (C_{OL}) and, Utility Cost (C_{UT}).

$$OPEX = 1.235\ (C_{UT}) + 2.735\ C_{OL} + 0.180\ CAPEX \tag{22}$$

As the CAPEX is the complete plant cost, it is amortised over the lifetime of the plant. Twenty-five years as the plant life is considered. However, the CAPEX can be annualised by considering a certain inflation rate according to the equation below.

$$CAPEX_a = CAPEX \frac{i(1+i)^n}{(1+i)^n - 1} \tag{23}$$

where $CAPEX_a$ is the annuity cost (€), i is the inflation rate (6.5%) [54] and n is the number of years of annuity interest.

Capture cost can be defined thanks to the annuity of the CAPEX and the OPEX.

$$Capture\ cost\ (€/t_{CO_2}) = CAPEX_a + OPEX \tag{24}$$

2.5. Environmental analysis

The main environmental impact indicator for carbon capture is the CO_2 emissions avoided to evaluate and quantify the effect on global warming. Usually, the CO_2 recovery reached for these systems is around 90%. In this work the performance of the CPU with a membrane can be higher. Two key performance indexes are to be considered: the CO_2 recovery of the system defined as:

$$CO_2\ recovery = \frac{\dot{m}_{CO_2\ captured}}{\dot{m}_{CO_2\ in}}.100 \tag{25}$$

and the CO_2 emissions avoided, which considers the CO_2 emissions due to the utility consumption according to:

$$CO_2\ avoided = \frac{\dot{m}_{CO_2\ captured} - \dot{m}_{CO_2\ utility}}{\dot{m}_{CO_2\ in}}.100 \tag{26}$$

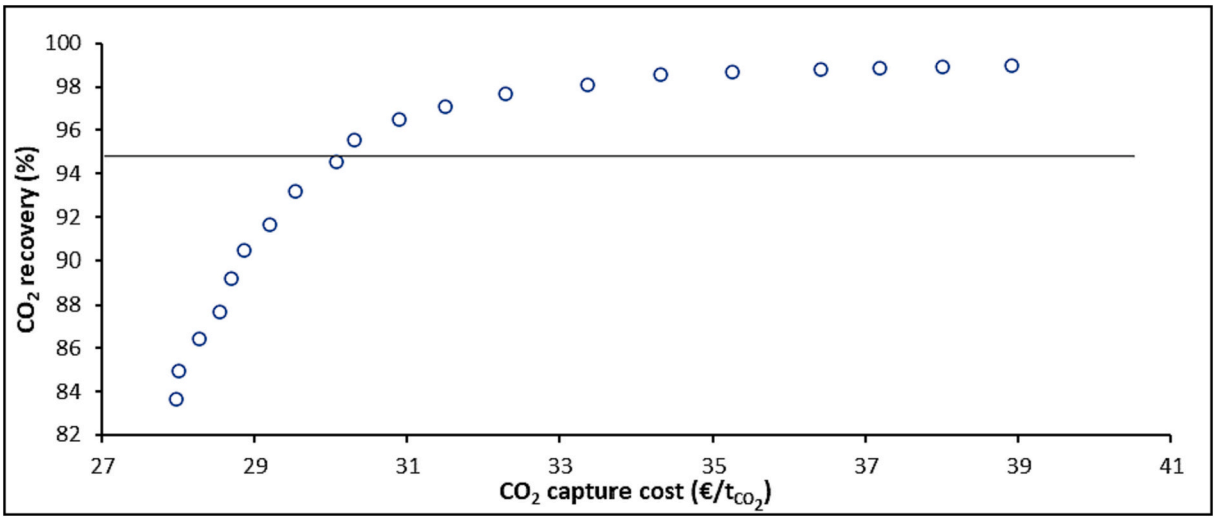

Fig. 7. Pareto front for optimisation of cost-recovery.

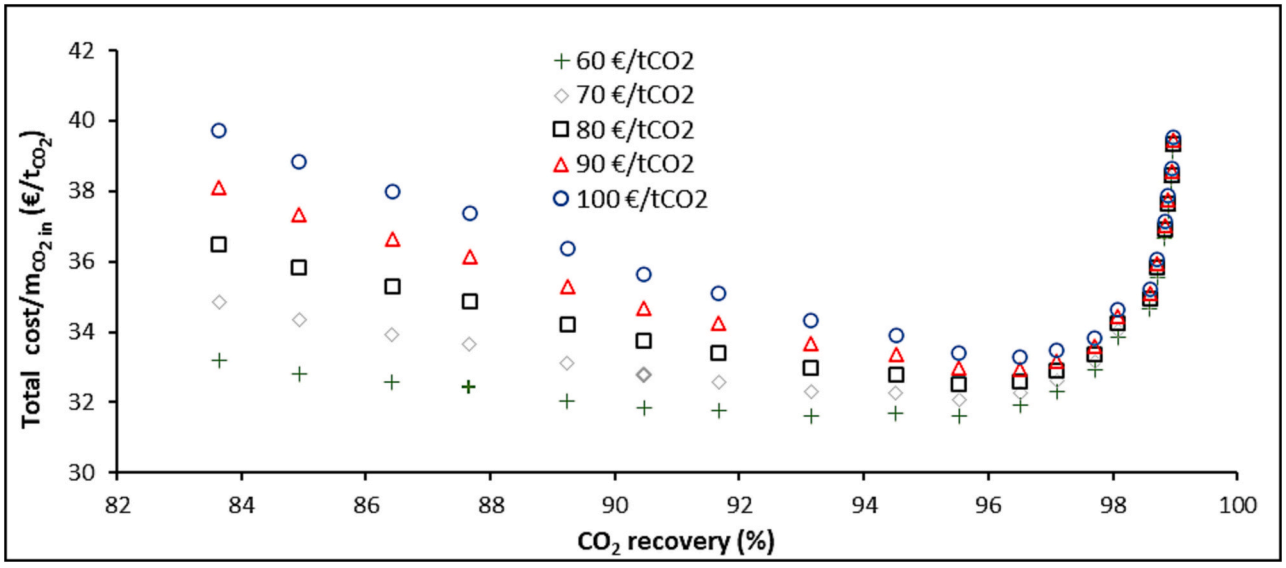

Fig. 8. Total CO_2 cost considering capture cost and carbon tax (see legend).

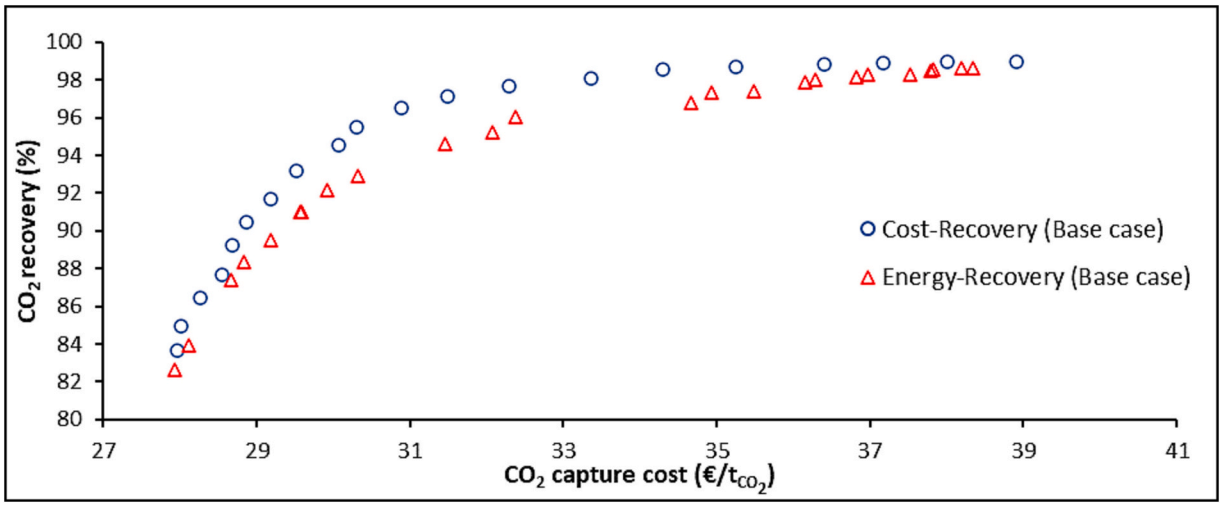

Fig. 9. Comparison between pareto front of cost-recovery and energy-recovery.

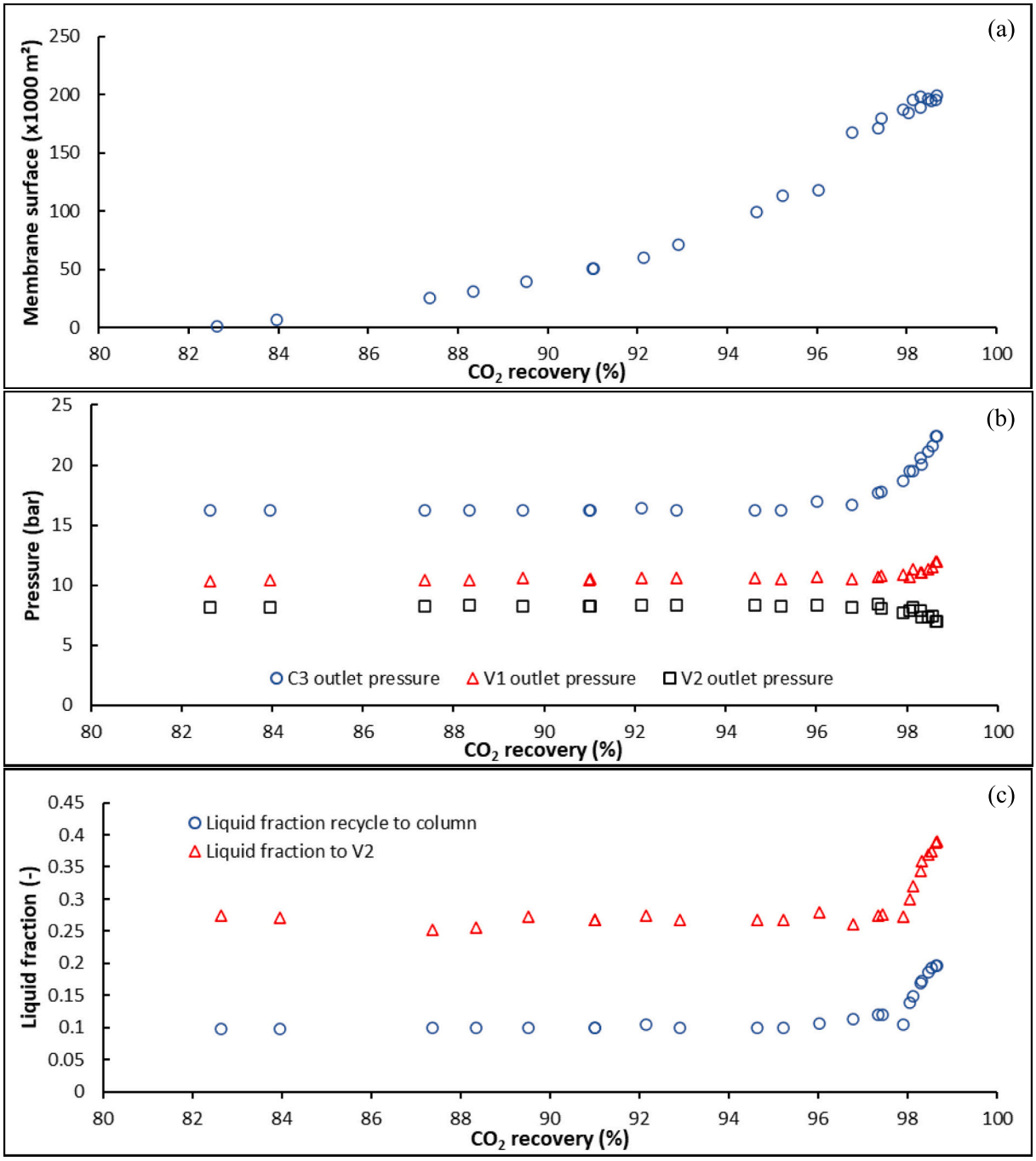

Fig. 10. Variable in function of the recovery for the base case (a) Membrane surface / (b) Pressure / (c) Liquid fraction.

3. Optimisation

3.1. Objective function

The KPIs of the economic, environmental, energy and exergy dimensions are relevant to evaluate the global performance of the process. The single variable analysis demonstrates that the CPU process can be optimised. This is the reason why in this work, a multi-objective optimisation is performed with the capture cost as a first objective function. The second and third objective functions consider the efficiency of the system for CO_2 emissions as well as the electrical consumption of the process. The fourth objective is the exergy efficiency of the system.

- Objective I: Capture cost (Eq. (24))
- Objective II: CO_2 recovery (Eq. (25))
- Objective III: Electrical consumption (Eq. (7))
- Objective IV: Exergy efficiency (Eq. (16))

To perform the optimisation, a system of variables has been defined. These variables are those identified in the process analysis. Table 7 includes the different variables as well as the limits imposed.

The system has constraints linked to the technical limits and to the operating conditions. Table 8 lists the different constraints implemented.

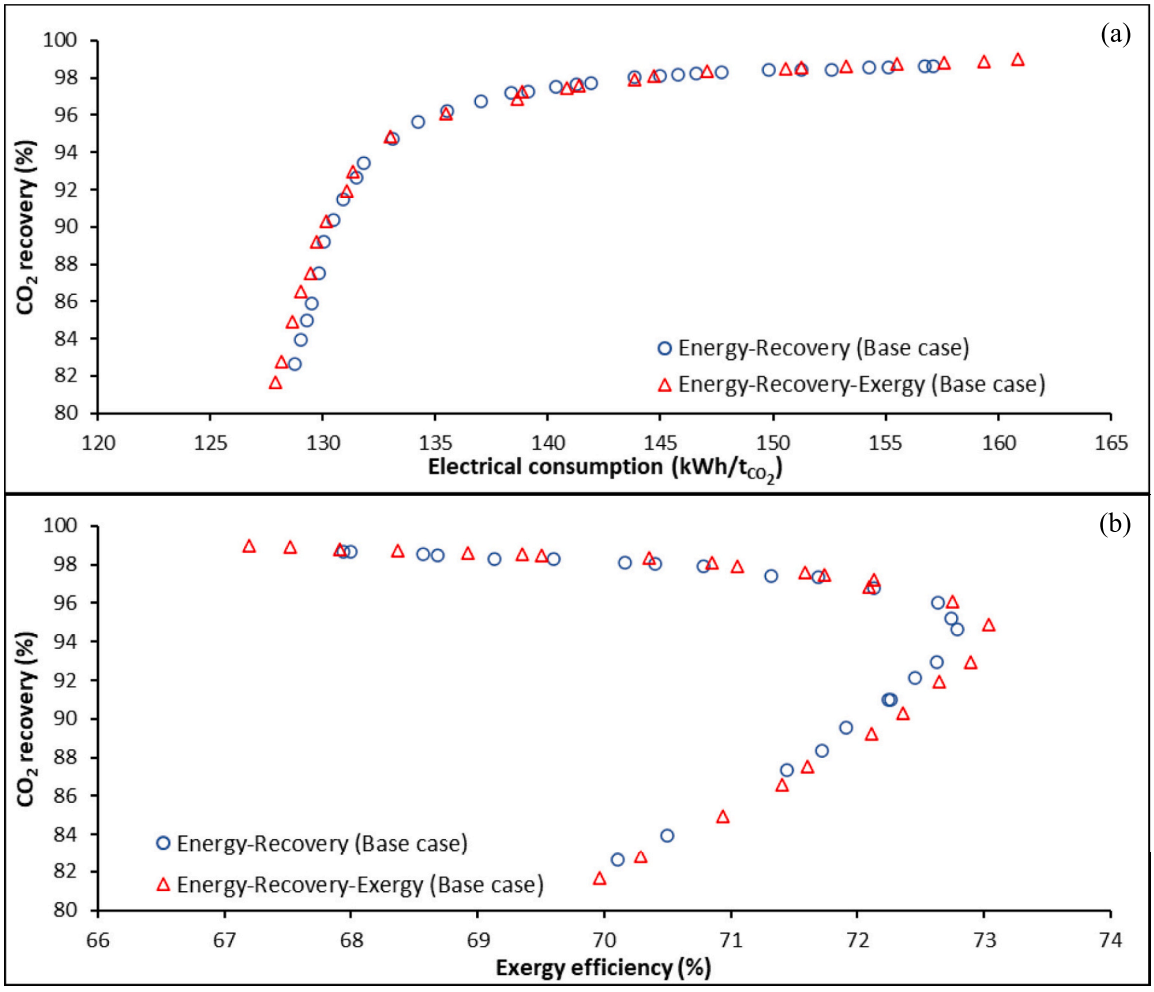

Fig. 11. Comparison between pareto front of energy-recovery and energy-recovery-exergy (a) Energy consumption function/ (b) Exergy efficiency function.

Table 11
Input variables and KPI for the three objectives optima of energy-recovery-exergy optimisation.

	Unit	Maximum recovery	Maximum exergy	Minimum energy
Input variable				
Discharge pressure of compressor C3	bar	23.97	16.39	15.75
Pressure of the valve V21	bar	12.87	10.50	10.03
Pressure of the valve V2	bar	7.44	9.19	8.99
Mass fraction towards L1CO2	-	0.15	0.12	0.11
Mass fraction towards L3CO2	-	0.46	0.35	0.36
Membrane area	m^2	200,000	101,000	1000
Discharge pressure of compressor C1	bar	2.31	2.63	2.52
Tower DES1 height	m	20.00	10.00	10.00
KPI				
Capture cost	€/t_{CO2}	38.85	31.51	27.95
CO_2 recovery	%	98.99	94.89	81.69
Electrical consumption	kWh/t_{CO2}	160.87	132.97	127.90
Exergy efficiency	%	67.19	73.03	69.96

3.2. Genetic algorithm

The genetic algorithm (GA) [55], based on the principle of natural evolution of Charles Darwin, is used in this optimisation due to the non-linearity between the inputs of the CPU Aspen model and its results. In a system to be optimised, the best results will be used to calculate new points to converge towards an optimisation.

Starting from an initial population composed of several individuals being defined by variables (called genes), these are then grouped together as a set of variables which define a proposed solution of the problem (called chromosome).

The individuals are assigned a rank according to their fitness towards the problem. This ranking will allow the selection of the best individuals among the population who will generate chromosomes by cross-over, i.e. by taking a part of the genes from one parent and the other part from the other parent. After this stage, part of the child chromosomes can undergo a mutation on one of the genes corresponding to leave a local minimum. Finally, the algorithm will end when the population converges (Fig. 6).

This method allows, among other things, individuals to be generated in a random way, which can be shifted with respect to the temporary minimum to increase the probability of leaving a local minimum. An advantage of GA is that the search for the minimum can be done either with a mono-objective or multi-objective function. A modified NGSA-II algorithm [56] is used in the context of CPU multi-objective optimisation. The genetic algorithm parameters are given in Table 9. The stopping condition is triggered when the function tolerance is less than the mean spread when the maximum stall generation is over.

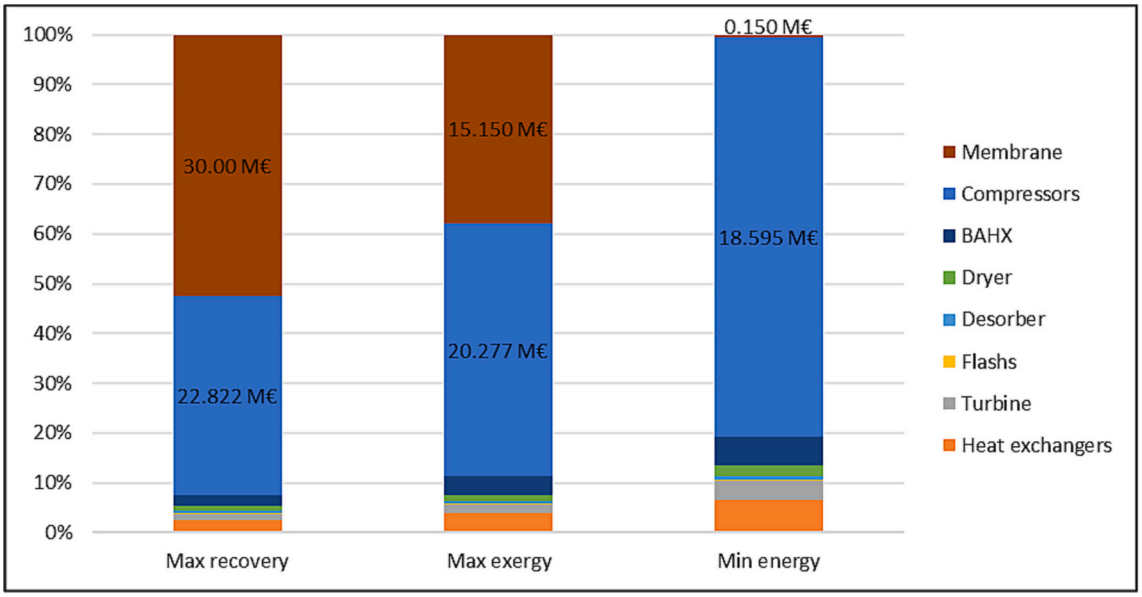

Fig. 12. Comparison of the CAPEX between the three optimised points.

Table 12
Comparison of the exergy destruction (kW) and its affectation (%) to the different equipment's between the three optimised points.

	Maximum recovery		Maximum exergy		Minimum energy	
Compressors	2481.7	22.14%	2202.0	27.77%	1972.3	28.95%
Heat exchangers	4979.9	44.43%	3896.3	49.15%	3362.3	49.35%
Turbine	139.8	1.25%	144.6	1.82%	239.4	3.51%
Desorber	128.3	1.14%	80.4	1.01%	60.0	0.88%
Dryer	32.7	0.29%	43.0	0.54%	38.3	0.56%
BAHX	1393.3	12.43%	934.5	11.79%	1073.7	15.76%
Membrane	1534.8	13.69%	516.1	6.51%	7.4	0.11%
Valve	146.7	1.31%	50.4	0.64%	39.2	0.58%
Mixer	372.6	3.32%	60.9	0.77%	20.9	0.31%
Total Ex_D	11,209.7		7928.1		6813.5	
η_{ex}	67.19%		73.03%		69.96%	

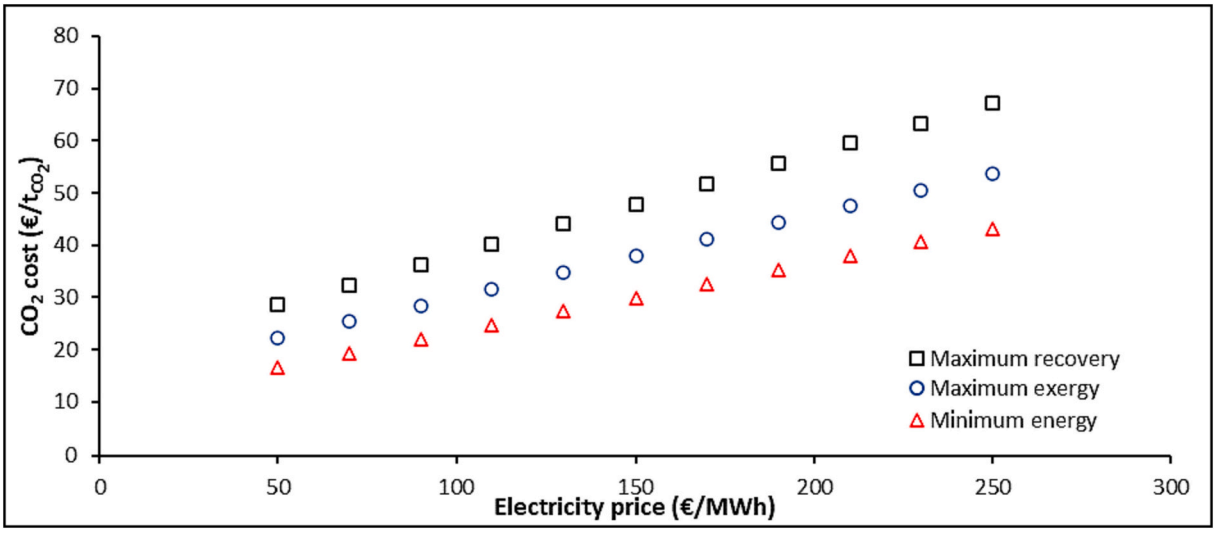

Fig. 13. Impact of the variation of the electricity price.

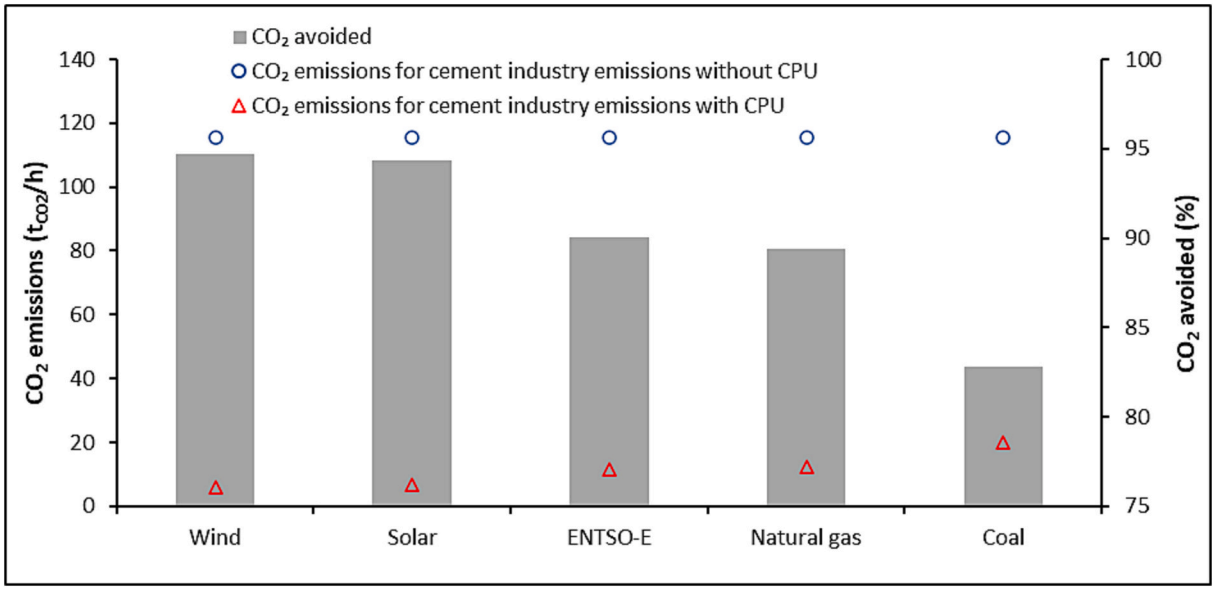

Fig. 14. CO_2 emissions and CO_2 avoided considering several sources of electricity production (Emissions factor of electricity (kg_{CO2e}/kWh): wind = 0.011; solar = 0.044; European Network of Transmission System Operators (ENTSO-E) = 0.399; Natural gas = 0.450; Coal = 1.000).

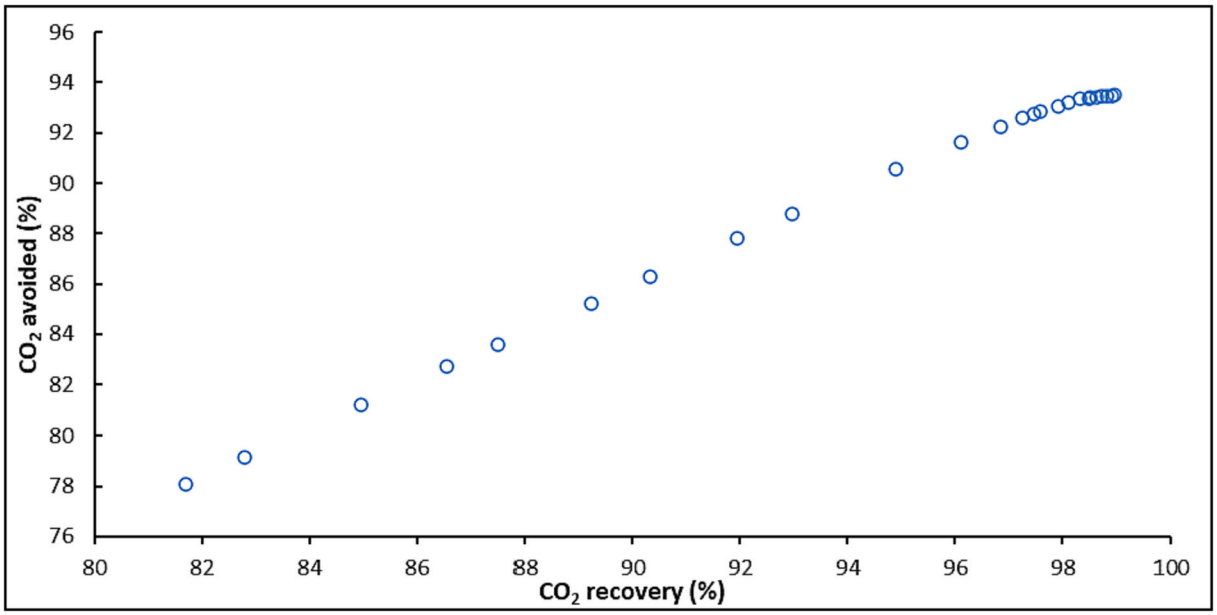

Fig. 15. Evolution of the CO_2 avoided in function of the CO_2 recovery for the base case optimisation.

3.3. Uncertainty quantification

Crude Monte Carlo Simulation is a state-of-the-art uncertainty quantification (UQ) method, randomly generating scenarios from the distributions on the input parameters until sufficient ($10^3 - 10^4$) values on the quantity of interest are collected to make a statistically sound distribution [57]. However, the method is computationally intractable for complex models. To increase the computational efficiency, a surrogate model of the system model for the space defined by the random environment can be constructed. Typical surrogate models include Kriging [58], support vector machines [59] and Polynomial Chaos Expansion (PCE) [60]. In the case of PCE, both the distribution parameters and the sensitivity indices (i.e., Sobol' indices) can be derived analytically from the coefficients that characterise the surrogate model. Rixhon et al. [61] used PCE to quantify the Sobol' indices on the cost of the future Belgian energy mix and highlighted the significant importance (53%) of the uncertainty related to the cost of e-fuels.

A UQ and global sensitivity analysis were performed to quantify the uncertainty on parameters and to identify the dominating parameter uncertainties. PCE is adopted being a surrogate-assisted UQ method that promises an improved computational efficiency when compared to usual Monte Carlo Simulation. To apply PCE to the system, the open-source Python framework RHEIA was used, developed by Coppitters et al. [62]. The PCE ($\widehat{M}$) replicates the input-output relation defined by the Aspen model (M) and consists of a truncated series of multivariate orthonormal polynomials Ψ, weighted by coefficients u:

$$\widehat{M}(\boldsymbol{\xi}) = \sum_{\boldsymbol{\alpha} \in \mathscr{A}^{d,p}} u_{\boldsymbol{\alpha}} \boldsymbol{\Psi}_{\boldsymbol{\alpha}}(\boldsymbol{\xi}) \approx M(\boldsymbol{\xi}) \tag{27}$$

where $\boldsymbol{\xi} = (\xi_1, \ldots, \xi_d)$ is a vector of the independent random parameters,

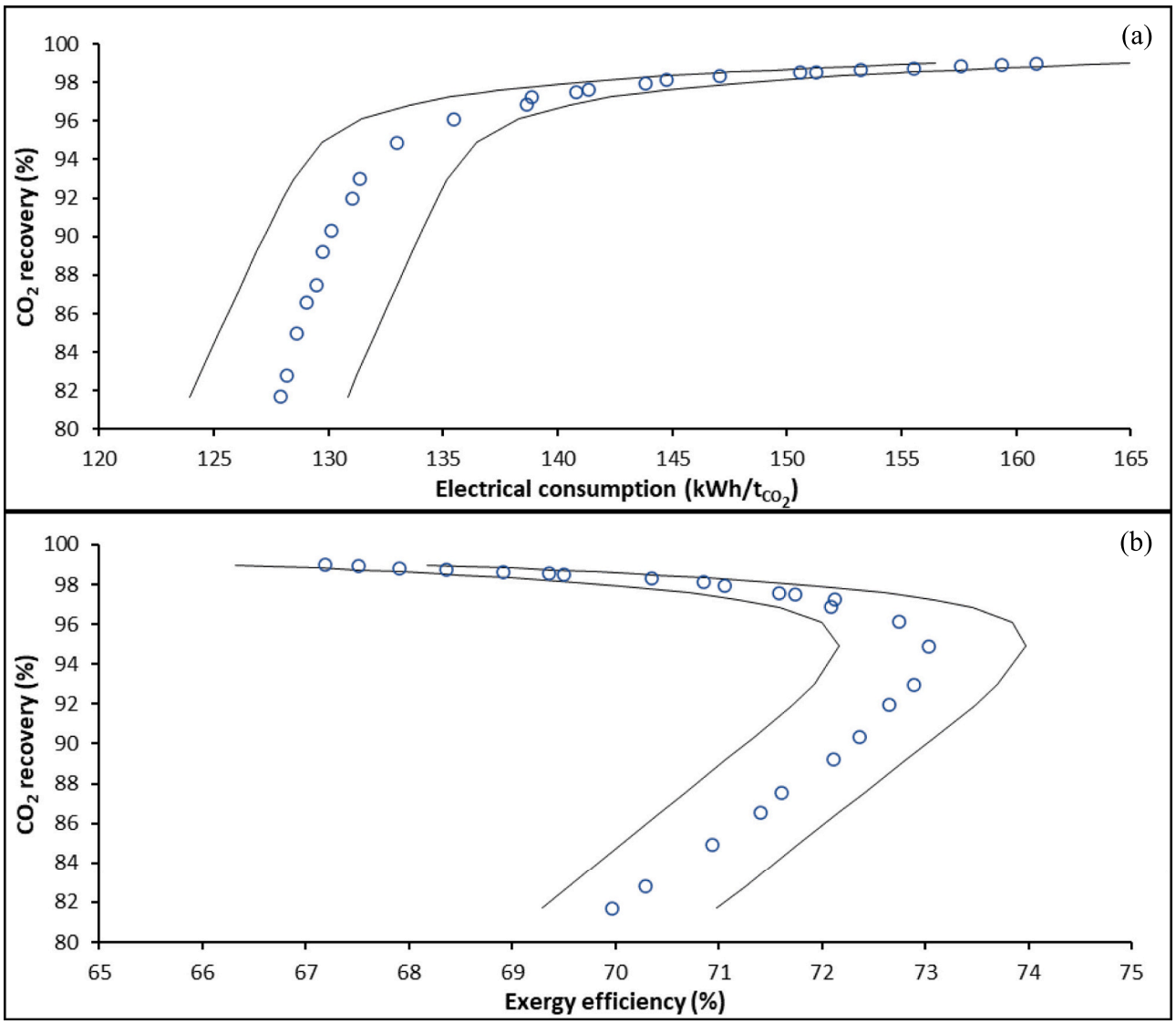

Fig. 16. Standard deviation (σ) for energy-recovery-exergy optimisation (a) Energy consumption function/ (b) Exergy efficiency function.

d corresponds to the number of input distributions and α is a multi-index. The truncation scheme limits the number of elements in the series $(P+1)$ based on a limiting polynomial order (p) and the number of uncertain parameters (d). The multivariate polynomial order is the sum of the order for each univariate polynomial in the multivariate polynomial (i.e., $|\alpha| = p$). Therefore, the multi-indices that correspond to an order below or equal to the limiting order are stored in the truncated series $\mathscr{A}^{d,p}$ [63]:

$$\mathscr{A}^{d,p} = \{\alpha \in N^d : |\alpha| \leq p\}. \tag{28}$$

The amount of existing multi-indices that comply with this rule equals [63]:

$$card(\mathscr{A}^{d,p}) = \left(\frac{p+d}{p}\right) = \frac{(d+p)!}{d!p!} = P+1 \tag{29}$$

To illustrate, for $d = 8$ and $p = 2$, 36 terms are present in the PCE. To quantify the coefficients (u), a regression method is adopted [63]. To acquire a well-posed least-square minimisation, two times the number of coefficients is defined as a sufficient amount of training samples [63]. Thus, $2(P+1)$ samples are evaluated in the Aspen model (M), and the model response for each quantity of interest is stored. The quasi-random Sobol' sampling technique is adopted to generate the training samples [64]. In this work, a polynomial order of 2 is required (72 training samples) to result in a Leave-One-Out error [63] below 1% of their value for the considered parameter.

Once the PCE is constructed, the statistical moments and sensitivity indices are quantified analytically from the PCE coefficients. Hence, no additional model evaluations are required to quantify the probability density function (PDF) and the sensitivity indices. From the coefficients, the mean μ and standard deviation σ are derived as follows:

$$\mu = u_0 \tag{30}$$

$$\sigma^2 = \sum_{\alpha \neq 0} u_i^2 \tag{31}$$

The sensitivity indices (i.e., Sobol' indices) identify the importance of the uncertain input parameter to the variability on the output. To be more specific, the total-order Sobol' indices (S_i^T) quantify the total impact of a stochastic input parameter on the performance indicator, including all interactions:

$$S_i^T = \sum_{\alpha \in \mathscr{A}_i^T} u_\alpha^2 \Big/ \sum_{i=1}^{P} u_i^2 \quad \mathscr{A}_i^T = \{\boldsymbol{\alpha} \in \mathscr{A} \mid \alpha_i > 0\} \tag{32}$$

where $\mathscr{A}$ is the set of all the PCE coefficients and α_i represents the co-

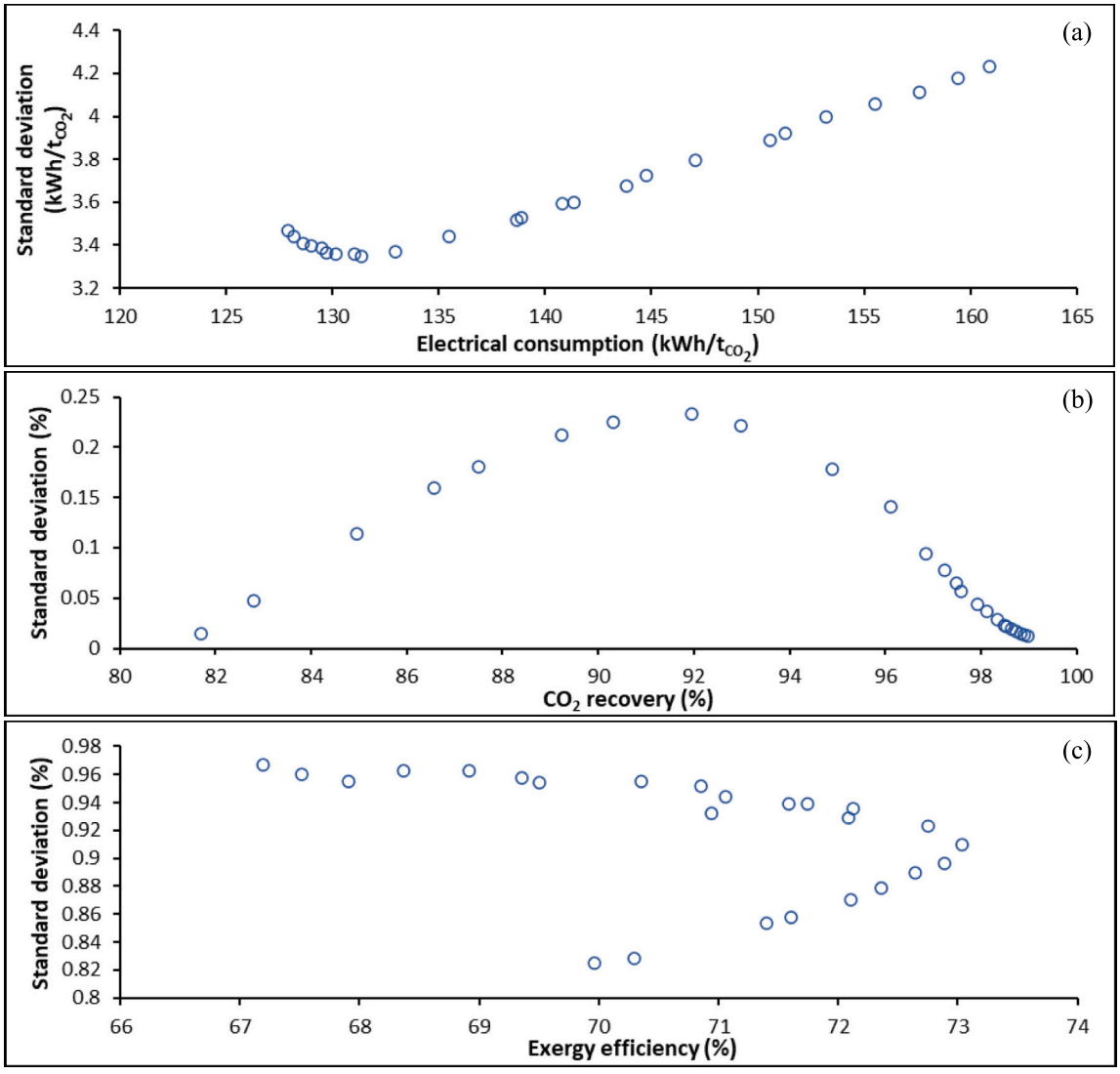

Fig. 17. Standard deviation (σ) value for (a) energy / (b) CO_2 recovery / (c) exergy.

Table 13
Different case studies considering CO_2 variations in the inlet flue gas.

Components	(Base case)	Case 1	Case 2	Case 3	Case 4
CO_2	79.0 mol%	64.0 mol %	69.0 mol %	74.0 mol %	84.0 mol %
CO_2 (Dry)	84.9 mol%	68.8 mol %	74.2 mol %	79.6 mol %	90.3 mol %
N_2	9.9 mol%	24.9 mol %	19.9 mol %	14.9 mol %	4.9 mol%
O_2	2.9 mol%				
Ar	1.2 mol%				
H_2O	7.0 mol%				

efficient related to the uncertain parameter *i*. As total-order Sobol' indices are considered, which consider both first-order and higher-order effects of the uncertain input parameters on the quantity of interest, the sum of the total-order Sobol' indices can be higher than 1.

In this CPU model, some values are taken from assumptions implying a possible divergence of results as well as a potentially large standard deviation. The purpose is to study this impact on the model and on the different optimised points. Thus, the parameters (Table 10) are varied according to uniform or Gaussian (uncertainty correspond to 3σ bound) functions to represent the potential deviation from the basic inputs. Gaussian probability distributions are chosen for fixed parameters with a high probability of being at the mean value such as permeability or heat exchanger pinch. Uniform probability distributions are taken for fixed parameters with equivalent probability for the different values.

4. Results and discussions

4.1. Multi-objective optimisation

A multi-objective optimisation was carried out on a CPU including a membrane-separation step to analyse the process with respect to the economic, environmental, energy and exergy dimensions.

Initially the optimisation considered only the objective functions I and II, capture cost and CO_2 recovery respectively. This optimisation allowed the evolution of the capture cost with respect to the CO_2 recovery to be shown. It is common to consider systems with a 90% capture rate. However, it is interesting to measure the financial impact of a higher capture rate. Fig. 7 presents the results of the optimisation. Up to 95% of CO_2 recovery, the additional cost compared to 90% is only 1.5 €/t$_{CO2}$. However, to reach a CO_2 recovery of 99%, the cost per tonne captured is increased by 9 € which corresponds to 30% of the cost to capture 90% of the CO_2.

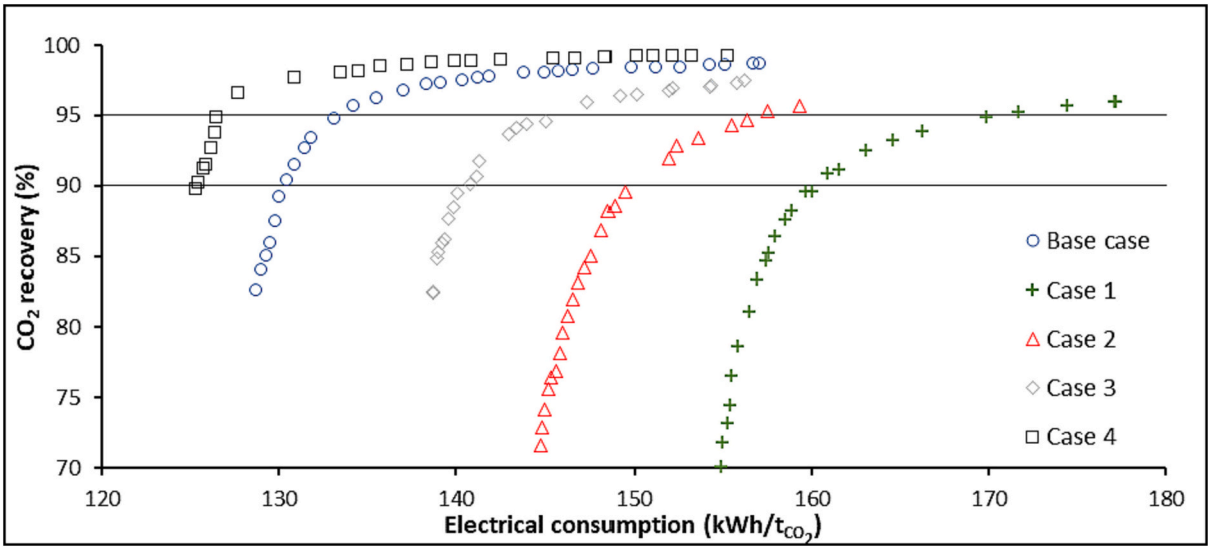

Fig. 18. Energy consumption and recovery for the different case studied.

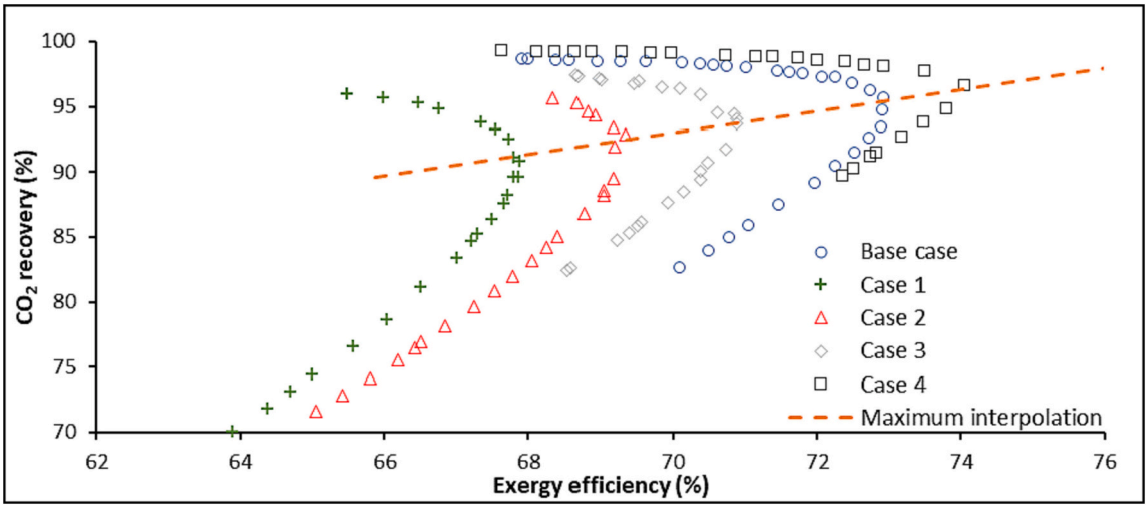

Fig. 19. Exergy efficiency and CO_2 recovery for the different cases.

Considering the carbon tax for uncaptured CO_2, an optimum can be determined for a CO_2 recovery value. Per tonne of CO_2 generated by the cement plant, the total cost, including the CO_2 capture costs and the carbon tax, can therefore be calculated as follows:

$$Total\ cost = \frac{CO_2\ recovery}{100} * CO_2\ capture\ cost + \frac{(100 - CO_2\ recovery)}{100} * carbon\ tax \quad (33)$$

Fig. 8 shows different curves depending on the value of the carbon tax. Thus, considering an interval of 60 to 100 €/t_{CO2} [3], a minimum of the total CO_2 cost for a 60 €/t_{CO2} carbon tax appears from a CO_2 recovery of 93% with a tendency towards a higher CO_2 recovery for a higher tax. For an allowance of 100 €, it is interesting to capture around 96.5% of the CO_2.

However, because of the uncertainties about the prices of energy carriers, it is also interesting to know how the cost behaves in relation to the energy-recovery optimisation. Fig. 9 shows a slight difference on the top for the energy-recovery optimisation because CAPEX is not optimised. However, as in the CO_2 capture cost, OPEX related to the electrical consumption is the dominant factor, it implies that a minimisation of the electrical consumption leads to a minimisation of the OPEX. In the continuation of this study, the optimisation is focused on the electrical consumption being independent of the electricity price.

Input variables related to energy-recovery optimisation results are shown in Fig. 10 (a/b/c). The CO_2 recovery is very dependent on the membrane and its operating parameters. Indeed, the increase of the membrane surface increases the CO_2 recovery (Fig. 10(a)). Moreover, to reach the highest CO_2 recovery, the differential pressure applied on the membrane is higher with an increase of the pressure in the cold box that increases the pressure of the vapour at the inlet of the membrane (Fig. 10 (b)). In this figure, the pressure at the outlet of the V2 valve decreases. This tendency is linked to a need to increase the cold duty, which is also reflected in the increase of the flowrate to this V2 valve for the second Joule-Thompson expansion (red triangle curve in Fig. 10(c)). The blue circle curve in Fig. 10(c) is the recirculation to the desorption column, which increases to maintain the purity above the required threshold in response to the rise in pressure at the outlet of the V1 valve (Fig. 10(b)) that feeds the column.

In a second step, a third objective optimisation of energy, recovery and exergy was established to study the behaviour of the latter. Fig. 11 (a) shows the CO_2 recovery as function of the electrical consumption for both optimisations considering in the first case the energy and recovery,

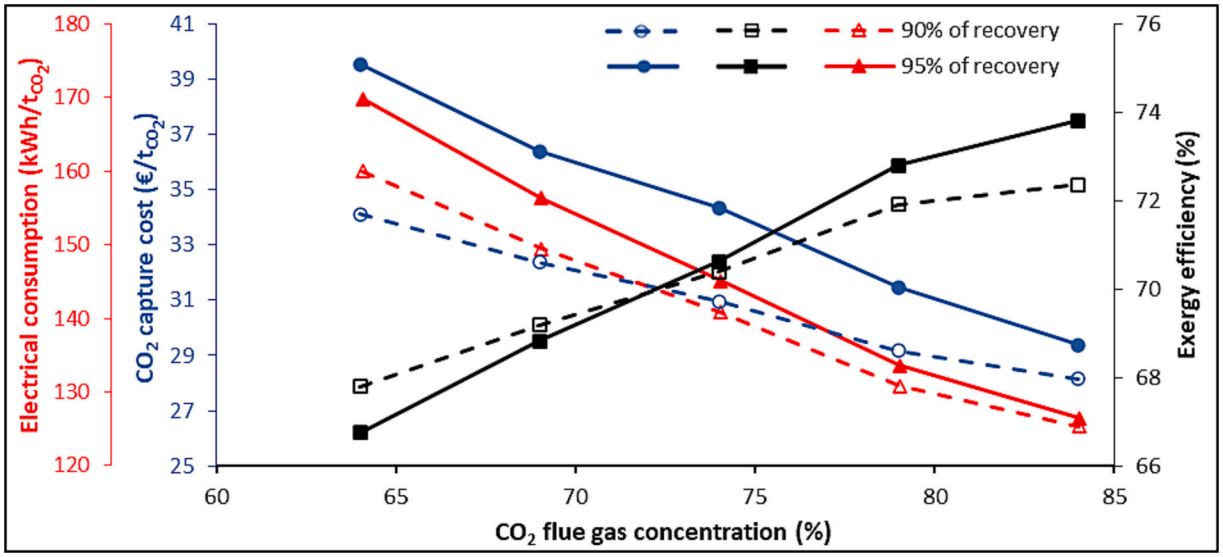

Fig. 20. Variation of the CPU electrical consumption, CO_2 capture cost and exergy efficiency as function of the CO_2 flue gas concentration for CO_2 recovery of 90% and 95%.

and in the second case the energy, exergy, and recovery. Results show that the electrical consumption is very similar in both cases. There is a little deviation when the exergy is considered around the maximum exergy (Fig. 11(b)).

It is interesting to note that for maximum exergy efficiency, the CO_2 recovery is around 95%. It is in this area that the CPU is most efficient. Table 11 presents the input variables and the KPI of the three objectives optima of the energy-recovery-exergy optimisation.

Concerning the capital cost, the main contributing cost is related to the compressor. This cost increases when the CO_2 recovery is higher as the pressure applied to the flue gas is higher and that of the Joule-Thompson expansion is lower. Depending on the CO_2 recovery reached, this amount decreases with the membrane cost that becomes a non-negligible cost at high CO_2 recovery. Indeed, the membrane goes from 1000 m^2 for the minimum recovery to 200,000 m^2 for the maximum recovery. The membrane and compressor contributions represent >80% of the total CAPEX, which varies between 23.2 M€ and 57.1 M€ for the lowest and the highest CO_2 recovery. Fig. 12 represents the distribution of the CAPEX for the different units.

Regarding the exergy analysis, the higher exergy destruction is induced by the heat exchangers, especially those that use the cooling water (around 50%). Compressors are the second unit that destroyed around 25% of the exergy, followed by the BAHX for which the exergy destruction varied in a range of 10–15%. Finally, the membrane exergy destruction depended on its surface and thus it increased with a higher CO_2 recovery. Table 12 provides the distribution of the exergy destruction between the units. Globally, the exergy efficiency (η_{ex}) is acceptable for such a process (between 67% and 70%). As a point of comparison, Jin et al. [17] had an exergy efficiency based on the same definition of 69.73% for their optimised point.

Overall, looking at the optimisation results for the base case, the CO_2 recovery should clearly be above 90%. Whether considering the overall capture cost and carbon taxes or purely in terms of system efficiency, CO_2 recovery tends to be around 95%. The comparison between the different cost-recovery, energy-recovery and energy-recovery-exergy optimisations shows that globally an energy-recovery optimisation gives very close results to the other two optimisations.

4.2. Sensitivity analysis

4.2.1. Electricity price variation

As already mentioned, electricity representing the highest energy contribution, it is necessary to evaluate the impact of its price on the capture cost. By varying the electricity price from 50 to 250 €/MWh, the evolution of the capture cost is linear. However, depending on the desired CO_2 recovery which implies a higher electrical consumption, the cost increases more significantly with the increase in the electricity price when seeking to achieve maximum recovery (Fig. 13). A higher electricity price is therefore not favourable for this process. Nevertheless, despite a price of 250 €/MWh, the capture cost in the case of exergy optimisation remains 53.74 €/t_{CO2}. In the more or less short term, the electricity price should decrease since the price of renewable electricity is between 30 and 110 €/MWh [65]. Considering this last value, the capture cost drop to 31.66 €/t_{CO2}. In summary, the electricity price and carbon tax which are two relatively variable elements, will have an influence on whether the capture system is sufficiently economically competitive to be implemented.

4.2.2. Environmental impact as function of the electricity source

As the process uses large amount of electricity as energy source, the source of the electricity will impact the overall balance of avoided emissions. The percentage of CO_2 avoided compared to an initial CO_2 recovery of 94.9% is 94.7% for wind power generation (0.011 kg_{CO2e}/kWh) and can degrade to 82.8% for coal power generation (1 kg_{CO2e}/kWh) (Fig. 14). In Europe (ENTSO-E), the electricity mix emits 0.399 kg_{CO2e}/kWh which gives an avoided CO_2 rate of 90.1%.

Taking emissions factor from the European electricity mix as an example, the impact of these emissions on the total carbon footprint of the process is not negligible. By looking at the CO_2 recovery, which is linked to the electrical consumption, this impact (Fig. 15) is less visible once the CO_2 recovery exceeds 97% due to the significant increase in electrical consumption compared to the small gain in terms of CO_2 recovery.

4.3. Uncertainty analysis

Compressors and turbines have a basic isentropic efficiency of 85% and 90%, respectively. This efficiency is dependent on the compressors and the gas passing through them. The impact on the compressors is shared between both compression chains (flue gas side and purified CO_2 side). A variation of +/− 5% is considered in this study. The other uncertainty analysed is the pinch at the cooling exchangers of the flue gas compression. This can vary for a given design if the flow rate or the gas composition changes. At the flue gas level, the oxygen from the

combustion exhaust can vary over time. A variation of 0.5% is considered to encompass the potential variations. The difference from the base case is reflected in the nitrogen concentration. The last uncertainties are posed on the membranes permeabilities which are experimental data defined on an installation. By applying a relative error of 10% following a Gaussian distribution, the uncertainty at the experimental level is represented.

The uncertainties on the results of the energy-exergy-recovery optimisation are quantified. The average standard deviation (σ) of the different results is 3.65 kWh/t_{CO2} for electrical consumption, 0.09% for CO_2 recovery and 0.92% for exergy efficiency. Fig. 16(a/b) show the standard deviation for energy and exergy respectively.

Standard deviation of objectives function is plotted on Fig. 17. Concerning the electrical consumption, a minimum of the standard deviation is present at around 132 kWh/t_{CO2}, meaning that more robust designs are present in this area (Fig. 17(a)). The Sobol' indices for electrical consumption illustrate that flue gas compressor efficiency and CO_2 compressor efficiency have the greater impact on the electrical consumption variation, with values around 0.70 and 0.25, respectively. Hence, providing a compressor map to the simulation is necessary to reduce the uncertainty on the electrical consumption. The other important contribution for the Sobol' indices come from the pinch in the exchangers with the cooling water. Permeability, oxygen concentration and turbine efficiency do not have a significant impact on the variation of the electrical consumption. These conclusions are noticed for the exergy variation, which is impacted mainly by these two same parameter uncertainties (Fig. 17(c)). Concerning the CO_2 recovery, only permeability uncertainty has an impact, with the highest Sobol' indices for CO_2 permeability equal to 0.98. Residues come from permeability of other components and O_2 concentration. Other parameters do not have an impact on CO_2 recovery. The standard deviation is very low for the extremity because the values are very close to the limit that involves this trend (Fig. 17(b)).

4.4. Optimisation considering several flue gas compositions

In this section, different flue gas compositions are considered to determine the impact on the process parameters. CO_2 can be more diluted due to a higher air entrance that degrades the high concentration obtained thanks to oxy-combustion conditions. Only the variation of carbon dioxide in the range of 64 mol% to 89 mol% and nitrogen were modified for this study (Table 13).

The more a gas is already concentrated in CO_2, the easier it is to separate the CO_2 from the other compounds, which leads to a lower electrical consumption. However, the optimum recovery varies according to the CO_2 concentration (Fig. 18). For a concentration higher than the base case, a CO_2 recovery higher than 95% is to be considered. Below the base case concentration, the optimum CO_2 recovery is between 90 and 95%. It is thus more interesting from an energetic point of view to capture >90% of the CO_2 from the flue gas.

Therefore, the optimal CO_2 recovery can be determined according to the maximum exergy efficiency. The exergy maxima are aligned as shown in Fig. 19, with a maximum exergy efficiency of 74% for Case 4 (CO_2 recovery of 95%).

Fig. 20 shows the evolution of the KPIs for a 90 and 95% CO_2 recovery considering different CO_2 concentrations in the flue gas. As shown in this figure, electrical consumption follows a very similar trend as for the capture cost. For a CO_2 concentration of 74%, the exergy efficiency shows that it is more energetically (and therefore economically) interesting to have a CO_2 recovery of 95%. As regards to the capture cost, the difference between both CO_2 recoveries decreases when the concentration in the flue gas is higher. A good maintenance of the process, thus avoiding the air inlets, can make it possible to have better performances for a slight difference from an economic point of view.

5. Conclusion

This work presents a detailed analysis of a carbon purification unit (CPU) designed specifically for treating flue gas coming from an oxy-combustion cement kiln. A cryogenic process coupled with membrane unit has been implemented to increase the global CO_2 recovery of the process, and to reduce the electrical consumption of cryogenic unit. This process has been studied through a 4E analysis concerning energy, exergy, economy, and environment. An optimisation with a genetic algorithm by minimising electrical consumption (at the same time to minimise capture cost) and by maximising the CO_2 recovery and exergy efficiency of the process is performed.

The study revealed an exergy maximum linked to CO_2 recovery, with higher values observed for CO_2-rich flue gases, reaching a maximum exergy efficiency of 73.03% for the base case. The capture cost exhibited a parallel trend with electrical consumption, aligning with CAPEX annualization between 1.6 and 4 €/t_{CO2}, depending on capture cost ranges and electricity prices. Below 100 €/MWh, the cost for a 95% CO_2 recovery is 30 €/t_{CO2} which is considered as acceptable, keeping in mind that it is only a part of the CCUS chain costs.

From an environmental point of view, this study shows that it is economically interesting to increase the capture rates compared to the usual 90% of CO_2 recovery, even decreasing the total costs related to the emission and capture of CO_2 according to the carbon tax. Since this is an electricity-only process, the source of electricity is important and can lead to a degradation of >10% of the CO_2 recovery for the most polluting sources.

Uncertainty analysis highlighted energy and exergy as the most affected aspects, with standard deviations of 3.65 kWh/t_{CO2} and 0.92% for exergy efficiency. Implementing a compressor map could reduce uncertainties, particularly for flue gas.

Additionally, the variation of the inlet gas CO_2 concentrations shows that the richer the flue gas, the more the electrical consumption decreases and the higher the exergy efficiency. The curves show a linearisation of the exergy maximum as a function of the CO_2 concentration indicating that beyond the base case, a capture of >95% is economically interesting.

The carbon purification unit with membrane to recover CO_2, comparing with other cryogenic processes developed in the literature, allows a significant reduction of electricity consumption. Kolster et al. [16] and Shah [21] have studied a high-purity CPU (with a column to desorb impurities) on a gas containing approximately 78 mol% CO_2 and with an almost 90% recovery. The energy consumed is 164 and 172 kWh/t_{CO2}, respectively. In this work, for such a concentration and recovery rate, the electricity consumption is about 140 kWh/t_{CO2}, representing an energy reduction of >15%.

It is therefore important to manage the air inlets in the flue gas to keep a good efficiency of the installation. In view of these observations, a perspective of this study could be to couple the CPU to an ASU and to determine the optimum energy according to the oxygen purity and thus the concentration of the flue gas at the inlet of the CPU.

CRediT authorship contribution statement

Alexis Costa: Writing – review & editing, Writing – original draft, Visualization, Software, Methodology, Data curation, Conceptualization. **Diederik Coppitters:** Software, Resources, Conceptualization. **Lionel Dubois:** Writing – review & editing. **Francesco Contino:** Writing – review & editing. **Diane Thomas:** Writing – review & editing, Supervision. **Guy De Weireld:** Writing – review & editing, Validation, Supervision, Conceptualization.

Declaration of Competing Interest

The authors declare the following financial interests/personal relationships which may be considered as potential competing interests:

Alexis COSTA reports financial support was provided by University of Mons Faculty of Engineering. Lionel DUBOIS reports financial support was provided by University of Mons Faculty of Engineering. Diederik COPPITTERS reports financial support was provided by UCLouvain, Institute of Mechanics, Materials and Civil Engineering.

Data availability

No data was used for the research described in the article.

Acknowledgements

The authors acknowledge the SPF Economie (Belgium) for funding the DRIVER project in the framework of the Energy Transition Fund program. The authors are also grateful to the European Cement Research Academy (ECRA) for its support.

Appendix A. Supplementary data

Supplementary data to this article can be found online at https://doi.org/10.1016/j.apenergy.2023.122431.

References

[1] Runge-Metzger A. A clean planet for all a European strategic long term vision for a prosperous, modern, competitive and climate neutral economy. 2018.
[2] Chauvy R, Meunier N, Thomas D, de Weireld G. Selecting emerging CO_2 utilization products for short- to mid-term deployment. Appl Energy 2019;236:662–80. https://doi.org/10.1016/J.APENERGY.2018.11.096.
[3] EMBER. Carbon price tracker. https://ember-climate.org/data/data-tools/carbon-price-viewer/; 2023 (accessed March 13, 2023).
[4] Theo WL, Lim JS, Hashim H, Mustaffa AA, Ho WS. Review of pre-combustion capture and ionic liquid in carbon capture and storage. Appl Energy 2016;183:1633–63. https://doi.org/10.1016/J.APENERGY.2016.09.103.
[5] Hu Y, Yan J. Characterization of flue gas in oxy-coal combustion processes for CO_2 capture. Appl Energy 2012;90:113–21. https://doi.org/10.1016/J.APENERGY.2011.03.005.
[6] Dubois L, Thomas D. Comparison of various configurations of the absorption-regeneration process using different solvents for the post-combustion CO_2 capture applied to cement plant flue gases. Int J Greenh Gas Control 2018;69:20–35. https://doi.org/10.1016/j.ijggc.2017.12.004.
[7] Brandl P, Bui M, Hallett JP, mac Dowell N.. Beyond 90% capture: possible, but at what cost? Int J Greenh Gas Control 2021:105. https://doi.org/10.1016/j.ijggc.2020.103239.
[8] Ben-Mansour R, Habib MA, Bamidele OE, Basha M, Qasem NAA, Peedikakkal A, et al. Carbon capture by physical adsorption: materials, experimental investigations and numerical modeling and simulations – a review. Appl Energy 2016;161:225–55. https://doi.org/10.1016/J.APENERGY.2015.10.011.
[9] Robeson LM. The upper bound revisited. J Membr Sci 2008;320:390–400. https://doi.org/10.1016/j.memsci.2008.04.030.
[10] Castel C, Bounaceur R, Favre E. Membrane processes for direct carbon dioxide capture from air: possibilities and limitations. Front Chem Eng 2021:3. https://doi.org/10.3389/fceng.2021.668867.
[11] Voldsund M, Gardarsdottir SO, De Lena E, Pérez-Calvo JF, Jamali A, Berstad D, et al. Comparison of technologies for CO_2 capture from cement production—part 1: technical evaluation. Energies (Basel) 2019;12:559. https://doi.org/10.3390/en12030559.
[12] Onyeaka H, Miri T, Obileke K, Hart A, Anumudu C, Al-Sharify ZT. Minimizing carbon footprint via microalgae as a biological capture. Carbon Capture Sci Technol 2021;1:100007. https://doi.org/10.1016/j.ccst.2021.100007.
[13] Xia L, Lenaghan SC, Zhang M, Wu Y, Zhao X, Burris JN, et al. Characterization of English ivy (Hedera helix) adhesion force and imaging using atomic force microscopy. J Nanopart Res 2011;13:1029–37. https://doi.org/10.1007/s11051-010-0091-3.
[14] Krzywanski J, Ashraf WM, Czakiert T, Sosnowski M, Grabowska K, Zylka A, et al. CO_2 capture by virgin ivy plants growing up on the external covers of houses as a rapid complementary route to achieve global GHG reduction targets. Energies (Basel) 2022:15. https://doi.org/10.3390/en15051683.
[15] Lockwood T. Developments in oxyfuel combustion of coal. IEA Clean Coal Centre; 2014.
[16] Kolster C, Mechleri E, Krevor S, Mac Dowell N. The role of CO_2 purification and transport networks in carbon capture and storage cost reduction. Int J Greenh Gas Control 2017;58:127–41. https://doi.org/10.1016/j.ijggc.2017.01.014.
[17] Jin B, Zhao H, Zheng C. Optimization and control for CO_2 compression and purification unit in oxy-combustion power plants. Energy 2015;83:416–30. https://doi.org/10.1016/j.energy.2015.02.039.
[18] Magli F, Spinelli M, Fantini M, Romano MC, Gatti M. Techno-economic optimization and off-design analysis of CO_2 purification units for cement plants with oxyfuel-based CO_2 capture. Int J Greenh Gas Control 2022;115:103591. https://doi.org/10.1016/j.ijggc.2022.103591.
[19] Luyben WL. Simple control structure for a compression purification process in an oxy-combustion power plant. AIChE J 2015;61:1581–8. https://doi.org/10.1002/aic.14754.
[20] Koohestanian E, Sadeghi J, Mohebbi Kalhori D, Shahraki F, Samimi A. New process flowsheet for CO_2 compression and purification unit; dynamic investigation and control. J Chem Chem Eng Res 2021;40:593–604. https://doi.org/10.30492/ijcce.2020.37779.
[21] Shah MM. Carbon dioxide (CO_2) compression and purification technology for oxy-fuel combustion. Oxy-fuel combustion for power generation and carbon dioxide (CO_2) capture. Woodhead Publishing Limited; 2011. p. 228–55. https://doi.org/10.1533/9780857090980.2.228.
[22] Jin B, Zhao H, Zheng C. Thermoeconomic cost analysis of CO_2 compression and purification unit in oxy-combustion power plants. Energ Conver Manage 2015;106:53–60. https://doi.org/10.1016/j.enconman.2015.09.014.
[23] Li H, Hu Y, Ditaranto M, Willson D, Yan J. Optimization of cryogenic CO_2 purification for oxy-coal combustion. Energy Procedia 2013;37:1341–7. https://doi.org/10.1016/j.egypro.2013.06.009.
[24] Phillips I, Tucker A, Granstrom P-O, Bozzini G, Gent C, Capello PJ, et al. Network technology: Guidance for CO_2 transport by ship. 2022.
[25] Chambron N, Terrien P. Capture de CO_2 par unité cryogénique sur une centrale de type gazéification intégrée à cycle combiné. FR2997866A3. 2014.
[26] Béasse G, Bourhy-Weber C, Daeden S, Granados L, Lockwood F, Moreschini P, et al. Callide oxyfuel project callide oxyfuel project results from the CPU. Ponferrada. 2013.
[27] Stanley MW. Selection and design, Butterwoths series in chemical engineering. Chemical process equipment. 1990.
[28] Thome J. Alpema - the standards of the brazed aluminium plate-fin heat exchanger manufacturers' association. 2021.
[29] Fanchon K. Modélisation d'un module de perméation en phase gazeuse pour utilisation dans le logiciel de simulation Hysys. UMons; 1998.
[30] Fernandes Rodrigues D. Model development of a membrane gas permeation unit for the separation of hydrogen and carbon. 2009.
[31] Gorissen H. Temperature changes involved in membrane gas separations. Chem Eng Process 1987;22:63–7. https://doi.org/10.1016/0255-2701(87)80032-6.
[32] Kulkarni S, Hasse D, Sanders E, Chaubey T. CO_2 capture by sub-ambient membrane operation. 2013.
[33] Hao J, Tanaka K, Kita H, Okamoto K-I. Synthesis and properties of polyimides from thianthrene-2,3,7,8-tetracarboxylic dianhydride-5,5,10,10-tetraoxide. J Polym Sci A Polym Chem 1998;36:485–94. https://doi.org/10.1002/(SICI)1099-0518(199802)36:3<485::AID-POLA12>3.0.CO;2-J.
[34] Laribi S, Dubois L, Duprez ME, De Weireld G, Thomas D. Simulation of the sour-compression unit (SCU) process for CO_2 purification applied to flue gases coming from oxy-combustion cement industries. Comput Chem Eng 2019;121:523–39. https://doi.org/10.1016/j.compchemeng.2018.11.010.
[35] Murciano LT, White V, Petrocelli F, Chadwick D. Sour compression process for the removal of SOx and NOx from oxyfuel-derived CO2. Energy Procedia 2011;4:908–16. https://doi.org/10.1016/j.egypro.2011.01.136. Elsevier Ltd.
[36] Chen H, Wu W, Chen D, Feng Y. Comparative study of carbon-deNOx process by different sewage sludge chars. Chemosphere 2023;318:137981. https://doi.org/10.1016/j.chemosphere.2023.137981.
[37] Deng Ansart, Baeyens Zhang. Flue gas desulphurization in circulating fluidized beds. Energies (Basel) 2019;12:3908. https://doi.org/10.3390/en12203908.
[38] Miller BG. Emissions control strategies for power plants. Clean coal engineering technology. Elsevier; 2011. p. 375–481. https://doi.org/10.1016/b978-1-85617-710-8.00009-1.
[39] Robinson DB, Peng D-Y. The characterization of the heptanes and heavier fractions for the GPA Peng-Robinson programs. Gas processors association; 1978.
[40] Lasala S, Chiesa P, Privat R, Jaubert JN. VLE properties of CO_2 – based binary systems containing N_2, O_2 and Ar: experimental measurements and modelling results with advanced cubic equations of state. Fluid Phase Equilib 2016;428:18–31. https://doi.org/10.1016/J.FLUID.2016.05.015.
[41] Privat R, Mutelet F, Jaubert J-N. Addition of the hydrogen sulfide group to the PPR78 model (Predictive 1978, Peng–Robinson equation of state with temperature dependent k_{ij} calculated through a group contribution method). Ind Eng Chem Res 2008;47:10041–52. https://doi.org/10.1021/ie800799z.
[42] Xu X, Privat R, Jaubert J-N. Addition of the sulfur dioxide group (SO_2), the oxygen group (O_2), and the nitric oxide group (NO) to the *E*-PPR78 model. Ind Eng Chem Res 2015;54:9494–504. https://doi.org/10.1021/acs.iecr.5b02639.
[43] Rezk A, Al-Dadah R, Mahmoud S, Elsayed A. Characterisation of metal organic frameworks for adsorption cooling. Int J Heat Mass Transf 2012;55:7366–74. https://doi.org/10.1016/J.IJHEATMASSTRANSFER.2012.07.068.
[44] Ghannadzadeh A, Thery-Hetreux R, Baudouin O, Baudet P, Floquet P, Joulia X. General methodology for exergy balance in ProSimPlus® process simulator. Energy 2012;44:38–59. https://doi.org/10.1016/j.energy.2012.02.017.
[45] Kotas TJ, Tadeusz J. The exergy method of thermal plant analysis. Butterworths; 1985.
[46] Szargut J. Chemical exergies of the elements. Appl Energy 1989;32:269–86. https://doi.org/10.1016/0306-2619(89)90016-0.
[47] Rivero R, Garfias M. Standard chemical exergy of elements updated. Energy 2006;31:3310–26. https://doi.org/10.1016/J.ENERGY.2006.03.020.
[48] Turton R, Shaeiwitz JA, Bhattacharyya D, Whiting WB. Analysis, synthesis, and design of chemical processes. Pearson Education, Inc; 2018.
[49] Maxwell C. Cost indices. https://www.toweringskills.com/financial-analysis/cost-indices/; 2022.

[50] Yang Y, Chen Y, Xu Z, Wang L, Zhang P. A three-bed six-step TSA cycle with heat carrier gas recycling and its model-based performance assessment for gas drying. Sep Purif Technol 2020;237:116335. https://doi.org/10.1016/J.SEPPUR.2019.116335.
[51] Linde. Aluminium plate-fin heat exchangers. n.d. 2023.
[52] EMBER. Wholesale electricity prices in Europe. https://ember-climate.org/data/data-tools/europe-power-prices/; 2023 (accessed July 17, 2023).
[53] StatBel. Statistique quadri-annuelle sur le coût de la main-d'oeuvre. n.d, https://statbel.fgov.be/fr/themes/emploi-formation/salaires-et-cout-de-la-main-doeuvre/cout-de-la-main-doeuvre#documents.
[54] Chauvy R, Dubois L, Lybaert P, Thomas D, De Weireld G. Production of synthetic natural gas from industrial carbon dioxide. Appl Energy 2020;260:114249. https://doi.org/10.1016/J.APENERGY.2019.114249.
[55] Goldberg David E. Genetic algorithms in search, optimization, and machine learning. Addison-Wesley Professional; 1989.
[56] Deb K. Multi-objective optimization using evolutionary algorithms: An introduction. 2011.
[57] Rubinstein RY, Kroese DP. Simulation and the Monte Carlo method. Hoboken, NJ, USA: John Wiley & Sons, Inc.; 2007. https://doi.org/10.1002/9780470230381.
[58] Deng Z, Hu X, Lin X, Che Y, Xu L, Guo W. Data-driven state of charge estimation for lithium-ion battery packs based on Gaussian process regression. Energy 2020;205:118000. https://doi.org/10.1016/J.ENERGY.2020.118000.
[59] Richard B, Cremona C, Adelaide L. A response surface method based on support vector machines trained with an adaptive experimental design. Struct Saf 2012;39:14–21. https://doi.org/10.1016/J.STRUSAFE.2012.05.001.
[60] Coppitters D, de Paepe W, Contino F. Robust design optimization of a photovoltaic-battery-heat pump system with thermal storage under aleatory and epistemic uncertainty. Energy 2021;229:120692. https://doi.org/10.1016/j.energy.2021.120692.
[61] Rixhon X, Limpens G, Coppitters D, Jeanmart H, Contino F. The role of electrofuels under uncertainties for the belgian energy transition. Energies 2021;14:4027. https://doi.org/10.3390/EN14134027.
[62] Coppitters D, Tsirikoglou P, de Paepe W, Kyprianidis K, Kalfas A, Contino F. RHEIA: robust design optimization of renewable hydrogen and dErIved energy cArrier systems. J Open Source Softw 2022:7. https://doi.org/10.21105/joss.04370.
[63] Sudret B. Global sensitivity analysis using polynomial chaos expansions. Reliab Eng Syst Saf 2008;93:964–79. https://doi.org/10.1016/J.RESS.2007.04.002.
[64] Coppitters D, Verleysen K, de Paepe W, Contino F. How can renewable hydrogen compete with diesel in public transport? Robust design optimization of a hydrogen refueling station under techno-economic and environmental uncertainty. Appl Energy 2022:312. https://doi.org/10.1016/J.APENERGY.2022.118694.
[65] International Renewable Energy Agency. Renewable power generation costs in 2021. 2022.